University of California
Santa Barbara

Applications of Koopman Operator Theory to Highway Traffic Dynamics

A Thesis submitted in partial satisfaction
of the requirements for the degree

Master of Science
in
Mechanical Engineering

by

Allan M. Avila

Committee in charge:

Professor Igor Mezic, Chair
Professor Jeffrey Moehlis
Professor Francesco Bullo

September 2017

The Thesis of Allan M. Avila is approved.

Professor Jeffrey Moehlis

Professor Francesco Bullo

Professor Igor Mezic, Committee Chair

Applications of Koopman Operator Theory to Highway Traffic Dynamics

by

Allan M. Avila

Acknowledgements

The author acknowledges his heavenly father Yahweh, his lord Jesus Christ and the Holy Spirit for having their love, guidance and blessing throughout his life. The author also acknowledges his terrestrial parents Otto and Miriam Avila and his siblings Edwin, Otto, and Amy Avila for their continuous love and support.

Abstract

Applications of Koopman Operator Theory to Highway Traffic Dynamics

by

Allan M. Avila

The ever-increasing demands on transportation systems have led to the need for a robust and universal method for the analysis and forecasting of vehicular traffic systems. Traditional methods are mainly model-based, that is, the analysis is performed by investigating a mathematical model that represents the target dynamics of a traffic system. On the other hand, contemporary efforts have focused on utilizing artificial intelligence (AI) to model or forecast vehicular traffic dynamics. Despite these large efforts, there is still no single best-performing method for the analysis and forecasting of vehicular traffic dynamics. This is due to the very well known fact that the unpredictable behaviors involved in a traffic system, like human interaction and weather, leads to a very complicated high-dimensional nonlinear dynamical system. Therefore, it is difficult to obtain a mathematical or AI model that explains all events and time evolution of vehicular traffic dynamics. Even if such a model could be attained, it would not lead to a robust and universal way of traffic analysis and forecast, due to its need of extensive parameter tuning. Thus, in contrast to the model or AI-based approach, it is necessary to develop data-driven methods that can identify dynamically important spatiotemporal structures of traffic phenomena. In this thesis, we demonstrate how the Koopman operator theory can offer a model and parameter-free, data-driven approach to accurately analyzing and forecasting traffic dynamics. The Koopman operator theory framework is a rapidly developing theory in dynamical systems that offers powerful methods for analyzing complex nonlinear systems. The effectiveness of this framework is demonstrated

by an application to the Next Generation Simulation (NGSIM) data set collected by the US Federal Highway Administration and the Performance Measurement System (PeMS) data set collected by the California Department of Transportation. By obtaining a Koopman mode decomposition (KMD) of the data sets, we are able to accurately reconstruct our observed dynamics, distinguish any growing or decaying modes, and obtain a hierarchy of coherent spatiotemporal patterns that are fundamental to the observed dynamics. Furthermore, it is demonstrated how the KMD can be utilized to accurately forecast traffic dynamics by obtaining a decomposition of a subset of the data, that is then used to predict a future subset of the data.

Contents

Chapter 1

Introduction

Traffic models can typically be characterized as microscopic, mesoscopic or macroscopic. All of these methods have had their own success at capturing certain traffic phenomena. However, a lack of consistency between simulated results and observed data has led to years of confusion and disagreement within the traffic physics community [21]-[24]. In this section, we describe the success and limitations of certain traffic models and the spatiotemporal patterns typically observed in measured traffic data.

1.1 Modeling of Traffic

Microscopic traffic models view traffic as a collection of individual particles traveling together. These models can be divided into classic models and artificial intelligence models [21]. Classic microscopic models utilize mathematical equations, typically ODE's, to update the state of each vehicle in time. These classic models include stimulus-response based models[1][2][6]-[9], collision avoidance models[10]-[12], desired headway based models[2] or psycho-physical models[13]-[16] On the other hand, artificial intelligence models utilize computer algorithms for updating the state of every vehicle. These methods include the fuzzy logic based models,[17][18] the neural network models[25][26] or models that utilize a combination of the two. [19][20]. The state of the art review

of [21] indicates that the major downfall of microscopic models is the need to store information for each vehicle, at all times. This causes the computation to scale with the number of vehicles on the road, often times rendering the model incapable of real-time implementation. Furthermore, these models are heavily dependant on several parameters that require tuning. In order to tune such parameters detailed vehicle trajectory data, like the NGSIM, is required but limited and costly to collect. The most simple to calibrate of these models are the stimulus based ODE models. Despite their low calibration requirements, these models are further criticized due to their assumption that drivers can detect small changes in their state and will instantly react to these changes upon detecting them. In reality, drivers respond to a stimulus only when the stimulus is beyond some threshold therefore, psycho-physical models have also been implemented however, these models require a greater amount of parameters to be tuned. Lastly, the fuzzy logic and neural networks or combinations of the two are hindered by the difficulty in determining the correct sets and rules of the fuzzy logic and the "black box" nature of neural network models.

Mesoscopic models view traffic as a gas or sand-like material and employ statistical mechanics to model vehicle behavior. These models do not specify the behavior of traffic in terms of individual vehicles but rather in a more aggregated form through probability density functions. The three well-known types of mesoscopic models are the headway distribution models[33] the gas kinetic (GKT) models[28][29] and the cluster type models [27]. The GKT models account for a majority of the mesoscopic models and have been successfully extended to the case of multi-lane highways [30], multi-class vehicle interaction [31] and a combination of the two [32]. The GKT models have also yielded useful theoretical results, where in the works of [33]-[37], GKT models have been used to derive macroscopic traffic equations. Despite there theoretical success, mesoscopic models have always received much criticism for the high number of variables involved in their formu-

lation, which also renders many of these models impossible for real-time implementation [22]. Lastly, much like the microscopic models these models also depend on parameters which require tuning.

Macroscopic models view traffic as a continuum and utilize fluid mechanics based PDE's to describe the spatiotemporal evolution of traffic density, flow, and velocity. The three types of macroscopic models are the first order, second order, and Helbing type models [33]. Among the earliest attempts at analytically modeling traffic were the efforts of [39], where the first order LWR model was defined and used to study traffic behavior. The LWR model is relatively simple to handle and theoretically sound, as it is a simple mass balance equation. Furthermore the LWR model has been shown to be capable of producing the traveling wave dynamics typically observed in traffic [44]. However, some of the criticism of first order models, as summarized in [45][24][22], are their inability to describe unstable flow regimes or traffic oscillations and their inability of capturing localized structures or spontaneous "phantom" traffic jams. In light of these of shortcomings, second order models which utilize a mass and momentum balance equation have been proposed.[40]-[43]. Second order models are capable of describing traffic oscillations and support unstable flow regimes but still possess inherent limitations. As outlined in [46] some of the limitations of second order models are their ability to produce backward traveling vehicles, the tedious and unstable numerical algorithms needed to solve these models and their ability to produce characteristic speeds that exceed the speed of the traveling wave, suggesting that perturbations propagate faster than traffic.Lastly, Helbing type models, like the nonlocal GKT model [33] are third order equations that which appends an equation for the variance of the velocity. Helbing type models have been shown to overcome many of the previously mentioned theoretical discrepancies in addition to having much success in reconstructing spatiotemporal patterns observed on German highways [47]. Additionally, the development of new integration methods has

also rendered them capable of real-time implementation. Unfortunately, even the most promising macroscopic models often times are tedious to solve numerically, possess inconsistencies with observed phenomena, and lack a parameter-free implementation. Lastly, despite being the easiest models to calibrate, a general consensus on a single correct macroscopic model is not yet clear.

1.2 Empirical Observations of Traffic

Over the years, there has been a large effort put towards collecting empirical highway data via either traffic cameras or magnetic sensors placed along the highway. Empirical highway data has allowed traffic scientists to identify some common spatiotemporal patterns that arise in traffic dynamics [45]-[49] [59]-[62]. Using the non-local GKT model the works of [47] identify five different spatiotemporal patterns possible in a traffic system. Their findings are verified by studying 160 days of traffic data collected over a 30 kilometer stretch of the German A5 highway near Frankfurt. The different patterns identified are the pinned localized cluster (PLC), moving localized cluster (MLC), stop and go waves (SGW), oscillating congested traffic (OCT), and homogeneous congested traffic(HCT). The SGW and the OCT according to [47] are almost indistinguishable without the proper data filtering techniques. In this work we will refer to both as simply traffic oscillations or waves. Among the various types of patterns that arise, traffic waves or oscillations are perhaps one of the most studied traffic patterns. Research efforts have primarily focused on extracting characteristic properties of these traffic waves from data. The properties of interest are the period of oscillation, speed of propagation, wavelength and amplitude. According to [34] [53] [54] there is no single characteristic period of oscillation found in traffic, but that typically observed periods are in the 4-20 minute range. These oscillations are also known to propagate with an average velocity of -9 ± 3 miles

per hour (MPH) according to [51] [56]-[59]. It is also found that these waves typically maintain their amplitude profile and propagate without spreading [60] [61].The exact cause of traffic waves is still an open topic although, empirical research has led to the proposal of several possible mechanisms. The works of [49] [63] provide evidence showing that lane changing maneuvers are key in the development of traffic oscillations. Additionally, aggressive driving behavior [66], a bi-stability mechanism [64],merging and diverging effects [62] and the boomerang effect [47] are also proposed mechanisms or contributors of traffic oscillations. Localized or pinned traffic phenomenon, corresponding to the PLC state, are typically found near bottlenecks like on/off ramps and do not propagate in space. The MLC however, does propagate in space and corresponds to what we refer to as a traveling traffic jam.

Typically, the noisy and spiky nature of traffic data makes it very difficult to extract patterns or characteristics of traffic waves from raw data alone [69] [47]. This problem has led scientists to propose several different methods for extracting the periods of oscillation. Such methods include the Mauch method [48] [71]-[73], statistical based methods and even simple visual inspection of data. Many of these methods lack objectivity in that they don't offer an objective way of extracting periods and since they also depend on parameters they also lack a sense of universality. By universality we mean that the proposed method or model should be capable of being readily applied to different highways, across the world, without the need for extensive calibration. More importantly, it should be robust in that the method should consistently yield accurate results when applied internationally. The first attempts at empirically characterizing the country-specific differences of traffic waves can be found in [68], where traffic data from the United States, United Kingdom, and Germany were empirically analyzed and compared. This international comparison was motivated by the fact that different countries have different rules for infrastructure, vehicle class mix, driving rules and even driver behavior. The findings

of [68] indeed confirm key differences in the periods of oscillation and speeds of propagation between the three countries. It is further stated how this country-specific dynamics of traffic will require the re-calibration of current models or the development of new and different models. This dilemma can only lead to at best a country-specific and at worst location-specific modeling of traffic. The goal of this paper is to present an efficient and robust data-driven method of accurately identifying, reconstructing, analyzing and predicting spatiotemporal traffic patterns without the need of a model. The outline of the paper is as follows. In section two we give a general description of the Koopman operator theory framework of dynamical systems and the details of the data-driven algorithms, in section three we give a description of the data sets studied, in sections four and five we demonstrate the effectiveness of our methods by applying them to the NGSIM and Caltrans PEMS data set.

Chapter 2

Background:Koopman Mode Decomposition

The Koopman operator is an infinite-dimensional, linear operator that acts on a Hilbert space of functions called the space of observables [87][88]. The spectrum of this linear operator (eigenvalues and eigenfunctions) is capable of capturing key dynamic characteristics of a linear or nonlinear dynamical system. Additionally, the Koopman modes, corresponding to a particular choice of observable function, allow one to reconstruct and predict the observed quantity. Together the triplet of Koopman eigenvalues, eigenfunctions, and modes yield the Koopman mode decomposition (KMD) of an arbitrary observable [89],[90]. The most appealing feature of the KMD is its ability to be readily applied to real-world situations via the data-driven algorithms that have been developed in [89],[90] and [105]-[112]. These algorithms utilize data or measurements to approximate the Koopman mode decomposition of the system. With the KMD in hand, one is able to identify any stable or unstable modes present within the dynamics. This methodology has already seen a wide range of success in many different areas like fluids, neuroscience, energy, chaotic systems, control, video imaging, climate and many other complex nonlinear systems [92]-[96]. In this section we will briefly outline further details of the Koopman operator theory framework and its algorithmic implementation, and refer the reader to

the references listed above for a more rigorous treatment of the theory.

2.1 Dynamical Systems and KMD

In what follows we consider a continuous time dynamical system whose state space (phase space) evolves on an N-dimensional smooth manifold $\mathcal{M}$. The dynamical system is assumed to have an invertible flow map $\phi_t : \mathcal{M} \mapsto \mathcal{M}, t \in \mathbb{R}$. Therefore, for any initial condition $a_0 \in \mathcal{M}$ its evolution under the dynamics at some later time t is given by $a_t = \phi_t(a_0)$.

Let $\mathcal{H}$ be a Hilbert space of functions and let U^t be the Koopman family of operators which compose the functions in $\mathcal{H}$ with the flow ϕ_t. Hence, for any function $f \in \mathcal{H}$ and time t the action of the Koopman operator on f can be expressed as follows.

$$U^t f(a_0) = f \circ \phi_t(a_0) = f(a_t) \tag{2.1}$$

We now move forward to discuss some of the spectral properties of the Koopman operator. First, we note that since the Koopman operator is infinite-dimensional, its spectrum may contain a continuous spectrum in addition to the traditional point spectrum of finite-dimensional operators. Assuming that the dynamical system contains only a point spectrum we have that for any $\psi \in \mathcal{H}$ that is an eigenfunction of U^t, at eigenvalue $exp(\lambda t)$ for $\lambda \in \mathbb{C}$, its evolution in time is as follows.

$$U^t \psi(a_0) = \psi \circ \phi_t(a_0) = exp(\lambda t)\psi(a_0) \tag{2.2}$$

Next, we say that a subspace $\mathcal{A} \subset \mathcal{H}$ is invariant to the dynamics if for any $f \in \mathcal{A}$, its image under the flow, $U_t f \in \mathcal{A}$ for any time t. In cases, where the Koopman eigenfunctions or a subset of them, form a basis for an invariant subspace of $\mathcal{H}$ we can represent any

function in that invariant subspace with the basis of eigenfunctions. Formally speaking, let $\Psi = \{\psi_i\}, i \in \mathbb{N}$ be a set of Koopman eigenfunctions, $\lambda = \{\lambda_i\}$ the set of associated eigenvalues and let $\mathcal{E}_\Psi = span(\Psi)$ be the Koopman eigenspace associated with the basis of eigenfunctions. Then the Koopman mode decomposition of any observable $f \in \mathcal{A}$ is given by the following expression.[89],[90]

$$U^t f(a_0) = f \circ \phi_t(a_0) = \sum_{i=1}^{\infty} \psi_i(a_0) exp(\lambda_i t)\mathbf{v}_i \tag{2.3}$$

where, $\mathbf{v}_i = P_{\psi_i}(f)$ is the i-th component of the projection of f onto $\mathcal{E}_\Psi$ and is called a Koopman mode. Although, together the triplet $(\Psi, \Lambda, \mathbf{v})$ yield the KMD of an observable, it is important to note that (Ψ, Λ) are intrinsic to the dynamical system where as the Koopman modes $\mathbf{v}_i$ are not. Namely, they depend on the choice of f and will change according to that choice.

We now discuss how Koopman modes arise in practice. Let m be the number of data snapshots acquired, let $x_i \in \mathbb{R}^k, i \in \{1, \ldots, m\}$ be a single data vector at time i and let $X \in \mathbb{M}^{k\text{x}m}$ be the $k \times m$ data matrix $\{x_1, \ldots, x_m\}$. In practice, by sampling a continuous time dynamical system at some rate T one obtains a discrete time observation of the system. Formally speaking, we have an observation mapping, $F : \mathcal{M} \mapsto \mathbb{R}^k$ where $F = (f_1, \ldots, f_k)$ is assumed to be an embedding of $\mathcal{M}$ into k-dimensional data space. Hence, for every data vector x_i, there exists a point $a_i \in \mathcal{M}$ such that $F(a_i) = x_i$ for all i and $a_i = \phi_i(a_1)$. We note that F is not unique in any way, and in the case of traffic any observable quantity like velocity, density or flow corresponds to a different observation map F_{Vel}, F_{Dens}, or F_{Flow}. Now assuming there exists an invariant subspace $\mathcal{A} \subset \mathcal{H}$ and that the components of F are in $\mathcal{A}$, we can obtain an expression for our observed data points by taking the Koopman mode decomposition of F component-wise as shown

below.

$$x_t = F(a_t) = U^t F(a_1) = \sum_{i=1}^{k} P_{\psi_i}(F)\psi_i exp(\lambda_i t) \tag{2.4}$$

Where k is the number of linearly independent eigenfunctions (possibly infinite) needed to span $\mathcal{A}$. The $P_{\psi_i}(F)$ are the Koopman modes of the system that were introduced earlier.

2.2 Koopman Mode Decomposition: Algorithms

As stated previously, several algorithms for approximating the eigenfunctions, eigenvalues, and modes of the Koopman operator have been developed. In this paper, the results were obtained by utilizing the DMD algorithm developed in [99]. We briefly outline the details of the algorithm and its implementation to traffic data. We begin by taking the data matrix X, which contains m snapshots $x_i \in \mathbb{R}^k$in time.

$$X = \begin{bmatrix} x_1 & x_2 & \dots & x_m \end{bmatrix} \tag{2.5}$$

Then forming the two time-shifted matrices X_1 and X_2 as follows

$$X_1 = \begin{bmatrix} x_1 & x_2 & \dots & x_{m-1} \end{bmatrix}, \tag{2.6a}$$

$$X_2 = \begin{bmatrix} x_2 & x_3 & \dots & x_m \end{bmatrix} \tag{2.6b}$$

Now, what the DMD seeks to approximate is a k by k dimensional representation of the Koopman operator which satisfies the following relation shown below.

$$X_{k+1} = KX_k + r \tag{2.7}$$

Here K is a finite matrix representation of the Koopman operator, r is a residual error term due to the fact that we only have a finite-dimensional approximation of a possibly infinite expansion. On the other hand, in the case where a finite-dimensional invariant subspace of $\mathcal{H}$ does exist the dimension of the invariant subspace may actually be less than k. Utilizing (2.7) to rewrite (2.6b) as:

$$X_2 = \begin{bmatrix} | & | & \dots & | \\ Kx_1 & Kx_2 & \dots & Kx_{m-1} \\ | & | & \dots & | \end{bmatrix} + r = KX_1 + r \tag{2.8}$$

We then proceed by dropping the residual term and utilizing the singular value decomposition (SVD) of $X_1 = U\Sigma V^*$ to rearrange (2.8) as follows:

$$X_2 \approx KX_1 = KU\Sigma V^* \tag{2.9}$$

By rearranging (2.9) we obtain a matrix S that is related to K via a similarity transformation as shown below.

$$K \backsim \ S = U^* X_2 V \Sigma^{-1} \tag{2.10}$$

Since K and S are related their eigenvalues and eigenvectors are the same up to a similarity transformation. Hence if (λ_k, w_k) are an eigenpair of S then $(\lambda_k, v = Uw_k)$ is an eigen-pair of K. However, since (2.9) is the discrete time system associated to the original continuous time system, its eigenvalues $\{\lambda_k\}$ lie on the unit circle.Therefore the continuous time eigenvalues are given by $\omega_k = \frac{ln(\lambda_k)}{T}$ and the continuous time evolution of the observable $x_{kmd}(t)$ is given by the following expression.

$$x_{kmd}(t) = \sum_{i=1}^{k} b_0 v_i exp(\omega_i t) = V diag(exp(\omega t)) b_0, \tag{2.11}$$

Where $V = \{v_1, \ldots, v_k\}$ is a matrix whose columns are the eigenvectors v_i and b_0 is an initial amplitude coefficient associated with the initial data snapshot x_1, $b_0 = V^{\dagger}x_1$. Here † represents the Moore-Penrose pseudoinversoe of a matrix. Lastly, $diag(exp(\omega t)$ represents a diagonal matrix whose elements are $exp(\omega_i t)$. Next, one can evolve equation (2.11) for m time steps in order to reconstruct the observed data or by evolving past m time steps one can begin to predict the future state of the system. In this paper, we have applied this technique to traffic data and utilized the obtained eigenvalues and modes to identify, reconstruct, and predict spatiotemporal patterns that occur within the data.

Chapter 3

Traffic Data

In this section, we present the details of the Next Generation Simulation (NGSIM) data set collected by the Federal Highway Administration (FHA) and the Performance Measurement System (PeMs) data set collected by the California Department of Transportation (Caltrans). Both data sets are publicly available at `https://ops.fhwa.dot.gov/trafficanalysistools/ngsim.htm` and `http://pems.dot.ca.gov/`.

3.1 NGSIM Data

The NGSIM data set provides microscopic vehicle trajectory data for a 2100ft and 1640ft segment of the US 101 and US 80 highways respectively. Data for the US 101 highway was sampled at a frequency of 10Hz for 45 minutes between the hours of 7:50am-8:35am. A single on-ramp and off-ramp is present at approximately the 590ft and 1280ft locations. Data for the US 80 was sampled at the same rate but first for 15 minutes between the hours of 4:00pm-4:15pm and again for thirty minutes between the hours of 5:00pm-5:30pm. Only an on-ramp at approximately 400ft is present within the studied section for the US 80 highway. The US 101 consists of five main lanes and one auxiliary lane between the ramps whereas the US 80 consisted of six mainlines including a high occupancy lane.

Since we are interested in predicting and identifying spatiotemporal patterns we must construct macroscopic data from our trajectory data. To do this we implement the same binning methods utilized in [75] and developed in [74] to divide the spatiotemporal domain $[0, l]\times[0, t]$ into individual bins by $\text{bin}_{i,j} = ([i\Delta x, (i+1)\Delta x] \times [j\Delta t, (j+1)\Delta t])_{i\in(1\ldots n_x), j\in(1\ldots n_t)}$. Where $n_x = \frac{l}{\Delta x}$ and $n_t = \frac{t}{\Delta t}$ are the number of bins in space and time.

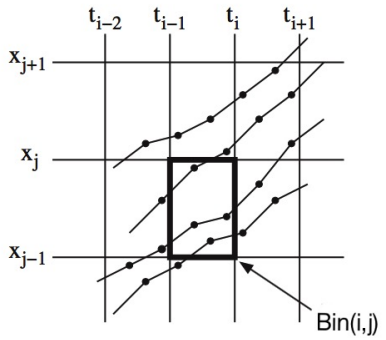

Figure 3.1: Adapted from Piccoli et al, Second-order models and traffic data from mobile sensors,. All copyright and ownership belongs to [74]

The binning formulas below were implemented with $\Delta x = 20$ ft/bin and $\Delta t = 5$ sec/bin. Later, in section 4 we address the sensitivity of our methods to this the choice of aggregation window. The quantities of interest (velocity, density or flow) are assumed constant in each bin and that trajectories leave a trace over these space-time bins.

$$\hat{V}_{i,j} = Mean_{trace\in bin_{i,j}}(V(trace)) \tag{3.1}$$

$$\hat{\rho}_{i,j} = \frac{Card(\{trace|trace \in bin_{i,j}\})}{\text{Numlanes } \Delta x\Delta t \text{ Sampling Rate}} \tag{3.2}$$

$$\hat{Q}_{i,j} = \hat{V}\hat{\rho} \tag{3.3}$$

Where $Card$ is the cardinality of a set.

As mentioned, the data collected for the US 101 highway was taken for a forty-five minute interval during 7:50am to 8:35am however, the data for the US 80 highway was collected for a fifteen minute interval during 4:00pm to 4:15pm and again for thirty minutes during 5:00 pm to 5:30 pm this leads to the construction of three separate data sets. Figures 3.2a-3.2c show a contour plot of the constructed velocity data sets for both highways. Where position along the highway is along the vertical axis and time runs along the horizontal axis. Plots of the constructed density and flow quantities can be referenced in the appendix.

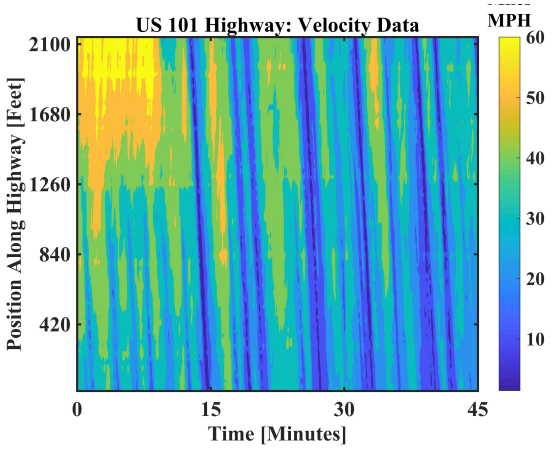

(a) US 101 Highway

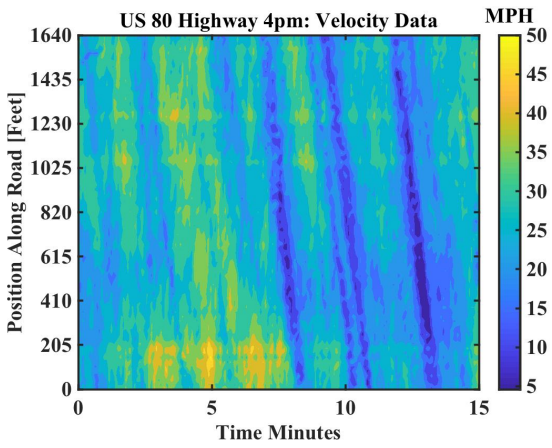

(b) US 80 Highway 4:00 pm

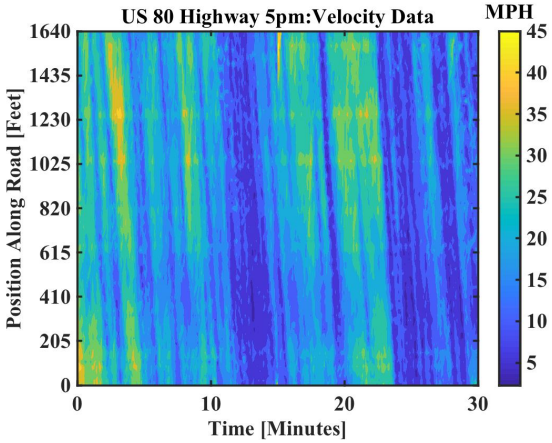

(c) US 80 Highway 5:00 pm

Figure 3.2: Velocity Contour Plot

Figures 3.2a-3.2c all exhibit these blue stripes of low velocities corresponding to traveling traffic jams. These features seem to propagate with constant speed and do not decay in amplitude or spread in waveform as they pass the on/off ramps (680ft and 1280 ft). Figure 3.2a demonstrates a noticeable region of high-speed, free-flowing traffic which occurs at the beginning of time (first 15 minutes) near then end of the highway section (1260ft-2100ft). This pocket of high-flowing traffic is present for about the first 12-15 minutes until the first traffic jam begins to propagate into our area of study. Also, during these first 15 minutes, the 0-1260 feet section experiences a series of small amplitude os-

cillations and can be seen as the group of faint light blue stripes that precede the jam. It is apparent how binning of the NGSIM's detailed trajectory data leads to a construction of macroscopic data rich with many different spatiotemporal features. For this reason, we utilize the NGSIM data to primarily study the effects of on/off-ramps by identifying key coherent spatiotemporal patterns.

3.2 PeMS Data

PeMS is an Archived Data User Service (ADUS) that provides over ten years of California highway traffic data. The state of California traffic network is divided into 11 districts in PeMS. The system covers more than 30,000 miles in directional distance and utilizes more than 6,800 controllers, 41,000 detectors, and 16,000 traffic census stations. The data is collected in real-time and five-minute aggregates are made publicly available through the Caltrans website. In this work, we study daily, weekly and monthly traffic data of several different highways throughout California. Figure 3.3a below is a contour plot of one month's data for the US interstate 5 highway. The data spans 400 miles in the northbound direction from the US-Mexico border to the states capital city of Sacramento. This section of the interstate 5 highway runs through, in spatial order, the major cities of San Diego, Orange County, Los Angeles, and Sacramento. Figure 5.4a is a contour plot of one week's data for the US interstate 10 highway, the data runs over 100 miles in the eastbound direction from Los Angeles to Beaumont.

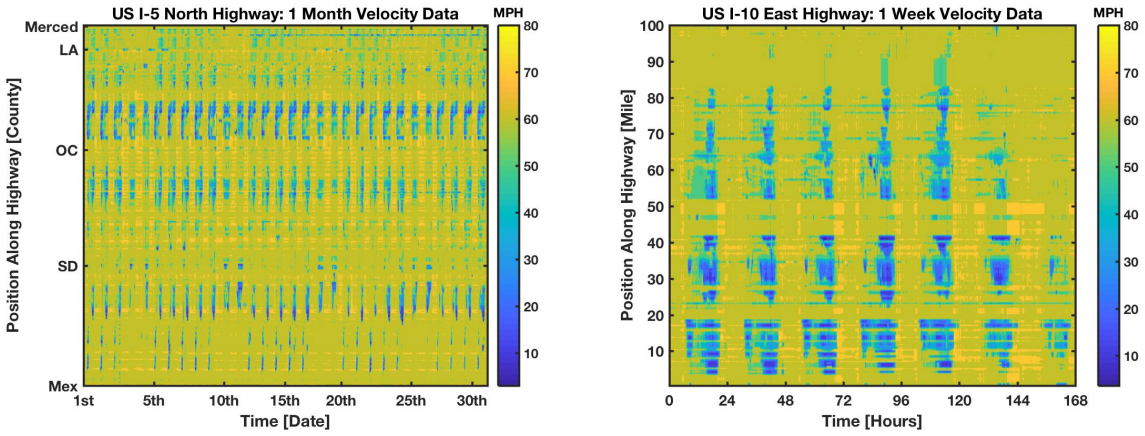

(a) Velocity Data for March 2017 of the US 5 Interstate Highway from the US-Mexico border to Sacramento

(b) Velocity Data for 03/06/17-03/12/17 of the US 10 Interstate Highway from the City of Santa Monica to Beaumont

Figure 3.3: Caltrans PeMs Data for the US I-5N and I-10E

The abundant historical data available and wide span of California's highway system renders the PeMS data set best for testing our forecasting schemes. Furthermore, the PeMS data is already provided in macroscopic terms and eliminates the need to bin trajectory data. Lastly, the PeMS data set is California's current system of performance measurement and therefore offers a more realistic setting for testing out forecasting schemes.

Chapter 4

Analysis of Traffic Data

In this section, we focus on demonstrating the KMD's success at accurately extracting and reconstructing spatiotemporal traffic patterns. We will first extract and identify dynamically important spatiotemporal patterns by analyzing the Koopman modes. Then we will reconstruct our data from the time evolution of the Koopman modes and analyze any discrepancies between the raw and reconstructed data.

4.1 Koopman Mode Analysis of NGSIM Data

Before proceeding, the issue of the aggregation window used in binning the data is addressed. We find that our methods can be sensitive to the choices of aggregation window Δx and Δt. In that, aggregation windows that lead to fat (more columns than rows) matrices often cause the matrix manipulations outlined in section 2 to be ill-conditioned and unstable results are obtained. This dilemma is addressed by utilizing the delay-coordinate embedding established by the Taken's embedding theorem [76]. Takens and others [79]-[81] have shown that under certain assumptions the attractor of the original dynamical system generating the data is recovered via this embedding. The relation below demonstrates how $l \in \mathbb{Z}^+$ time delays are obtained from the original m time snapshots. Now, since every original data vector x_i was in $\mathbb{R}^k$ our newly embedded

data vectors are in $\mathbb{R}^{lk}$. This allows us to obtain a taller matrix(more rows) than the original data matrix, at the expense of losing l time snapshots(columns).

$$\hat{X}_{delay} = \begin{bmatrix} x_1 & x_2 & \dots & x_{m-l} \\ x_2 & x_3 & \dots & x_{m-l+1} \\ \vdots & \vdots & \vdots & \vdots \\ x_l & x_{l+1} & \dots & x_m \end{bmatrix} \tag{4.1}$$

Note, how in this situation we are forced to aggregate the NGSIM data due to its Lagrangian nature. However, in practice one can encounter lengthy (weekly, monthly or yearly) data of only a few number of available sensors which will lead to a similar dilemma of a fat data matrix. This is indeed the case for the Caltrans PeMs data which we will utilize to test our forecasting schemes.

The method of correctly distinguishing dynamically important modes from numerical rubbish or noise is still an open problem within the Koopman operator community [111],[113]-[116]. In the context of traffic, we are guided by the fact that traffic oscillations are typically characterized by their timescale of oscillation (period). Therefore, in this work, we use the relations shown below to assign a timescale and growth/decay rate to each mode, and then sort them according to their these timescales.

$$\text{Timescale}(\psi_i) = \frac{2\pi}{Imag(\omega_i)} \tag{4.2}$$

$$\text{Rate}(\psi_i) = exp(Real(\omega_i)) \tag{4.3}$$

In addition to analyzing the velocity, flow and density alone we also compute the KMD of

these data sets simultaneously, by stacking our data sets into one tall matrix as follows.

$$\hat{X}_{VFD} = \begin{bmatrix} \hat{X}_{Velocity} \\ \hat{X}_{Flow} \\ \hat{X}_{Density} \end{bmatrix} \tag{4.4}$$

As mentioned in section two, the eigenvalues of the Koopman operator are inherent to the dynamics and do not depend on the choice of observable. Thus, we would expect to obtain similar timescales across the different choices of observables. Figure 4.1a is a stem plot of the first thirty or so timescales obtained for the US 101 highway. We can see how the timescales across different choices of observable cluster near each other as we would expect. However, it is still a bit difficult to say exactly which timescales or period we have identified. Now, if we first take the average of our data and subtract it out before embedding and decomposing, we can obtain much more agreement between the timescales, as shown in figure 4.1b. This mean subtraction of the data is motivated by the fact that the first continuous time eigenvalue of the Koopman operator is always equal to one, with zero imaginary part, and corresponds to the time averages of the data. Now since the goal of this section is to identify oscillations we seek to exclude or suppress this time average mode from our analysis since it carries no oscillatory information. We do this by averaging each row of our data matrix and subtracting that value from the corresponding row. In what follows the US 101 velocities and densities were mean subtracted before embedding using 7 delays.

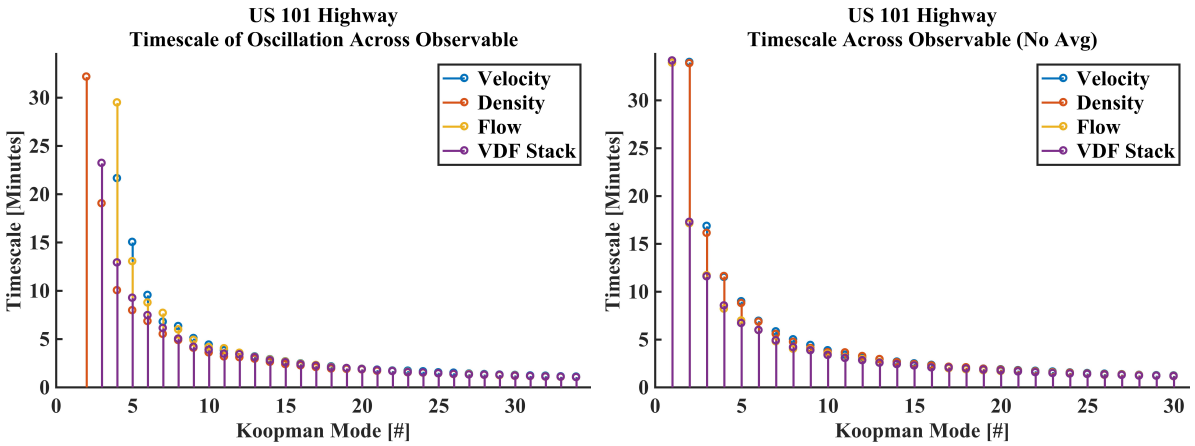

(a) Timescales Across Observables (b) Timescale Across Observables (No Avg)

Figure 4.1: US 101 Highway

In order to further demonstrate why we have chosen to subtract out our averages, we have plotted the first three modes with averages in figure 4.2a-4.2c. We can see how the first mode, figure 4.2a, corresponds to the time average. The second mode, figure 4.2b, seems to correspond to the early post off-ramp drop in velocities. However, the mode lacks an oscillatory form and has a purely real eigenvalue which indicates that this mode should correspond to the time average when evidently it does. The third mode, figure 4.2c, begins to look coherent but has some misshaped structure. By this, we mean that in the 0ft-1260ft section of the mode is slightly offset from the 1260ft to 2100ft section.

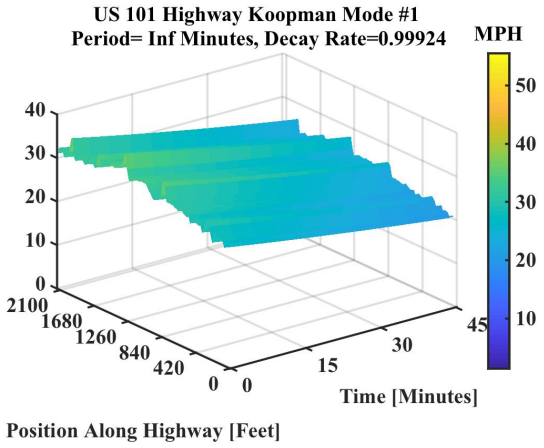

(a) Mode 1

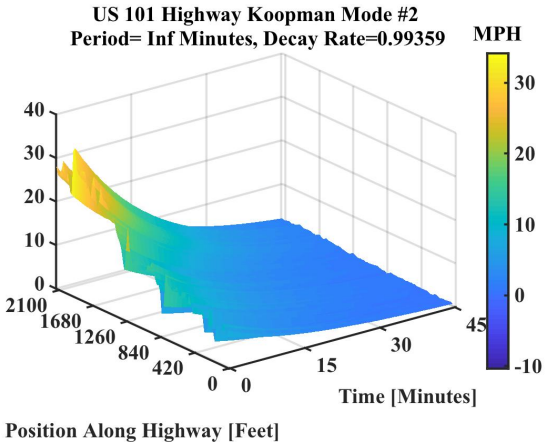

(b) Mode 2

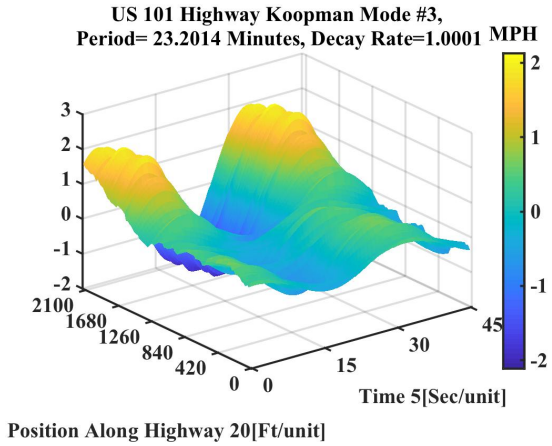

(c) Mode 3

Figure 4.2: First Three Modes With Averages

Now if we first subtract our averages before decomposing, we obtain Figures 4.3a-4.3b. It is clear from figure 4.3 that the first three modes all have complex eigenvalues and do not correspond to the time averages. Furthermore, the second and third modes are no longer misshaped and have physical significance.

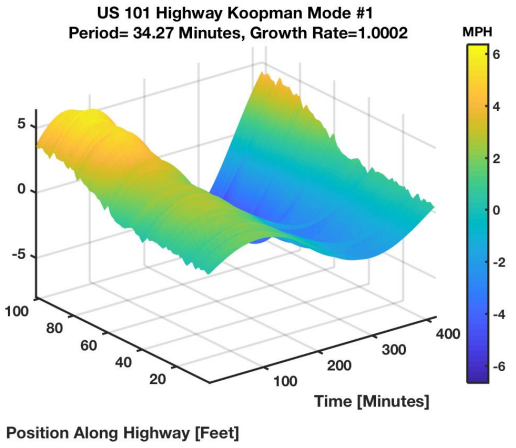

(a) Mode 1

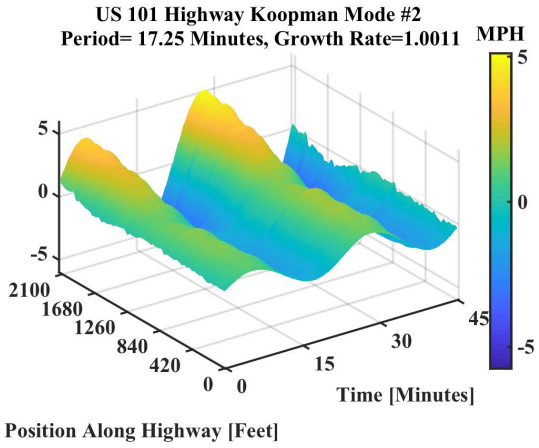

(b) Mode 2

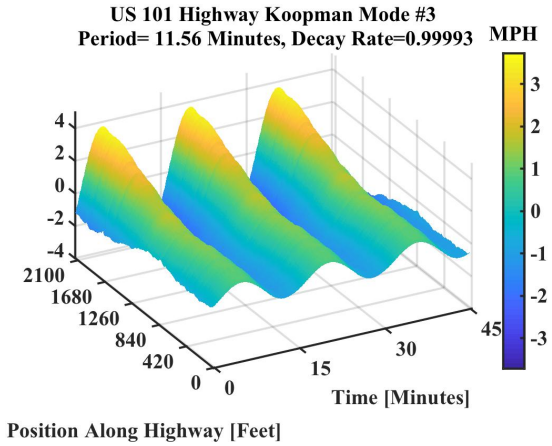

(c) Mode 3

Figure 4.3: First Three Modes Without Averages (on/off ramp at 680ft/1280ft)

Evidently, modes 1-3 all correspond to the initial transition of high to low velocities. These high period modes seem spatially restricted to the post off-ramp section of the highway (1280ft-2100ft). We can study the phase-locked properties of these modes by superimposing them and observing the construction and destruction in amplitude that takes place. Figure 4.4 contains plots of different superpositions between modes 1 through 3. In this figure, we can see how modes 1 and 2 superimpose constructively, figure 4.4a. However, modes 2 and 3 seem to be slightly out of phase everywhere, except the initial peak, figure 4.4b. Lastly, figure 4.4c illustrates the superposition of the all three modes

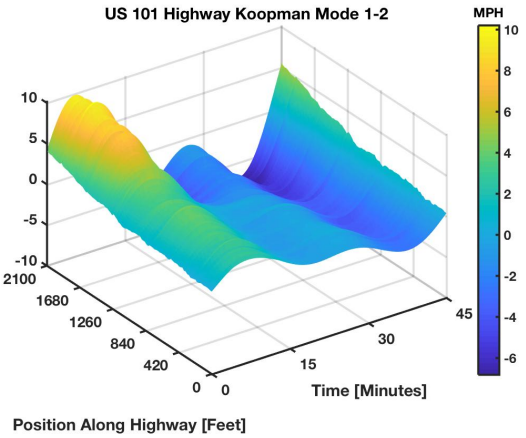

(a) Modes 1-2

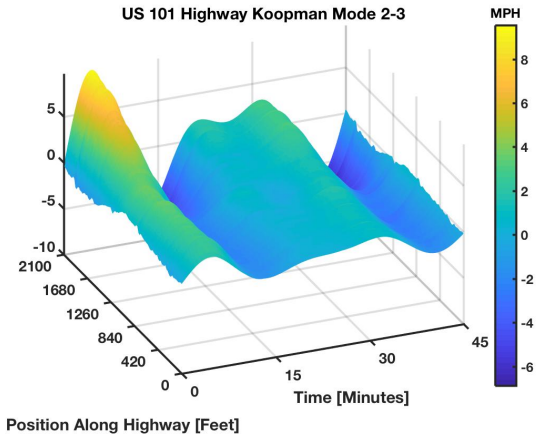

(b) Modes 2-3

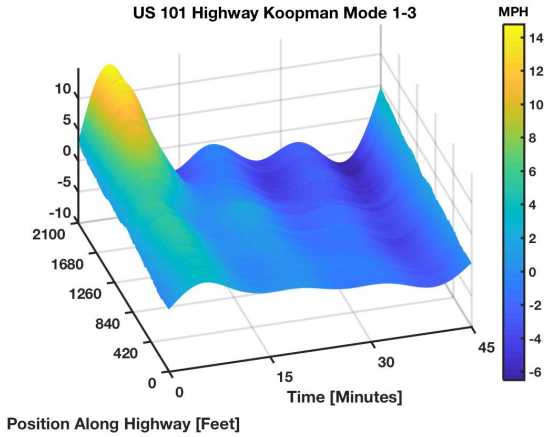

(c) Modes 1-3

Figure 4.4: Different Superpositions of Modes 1-3

which seems to better and better capture the high to low transition of velocities that occurs near the 15 minute mark.

Shown below in figures 4.5a and 4.5b is a plot of a top (speed vs time) and side (position vs time) view of the superposition of modes 2 and 3 previously shown in figure 4.4b. From figure 4.5a we can see how these modes are capturing not only the initial drop in velocities but also the propagating jams that occur near the 15 and 40 minute marks of the original data. Figures 4.5b and 4.5c show how the speed of propagation of these jams are not constant but rather change when propagating past the ramp section

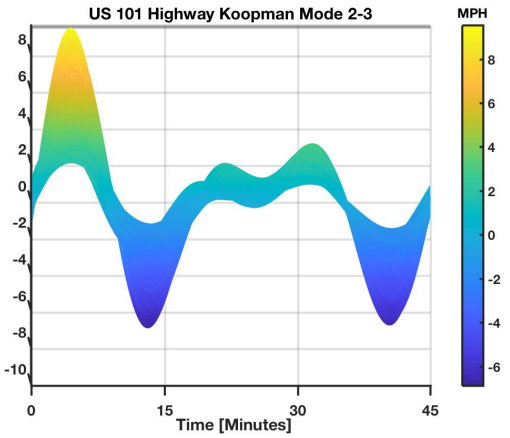

(a) Mode 2-3 side View

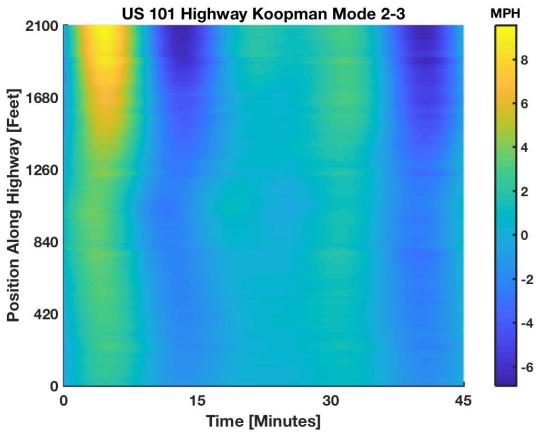

(b) Mode 2-3 Top View

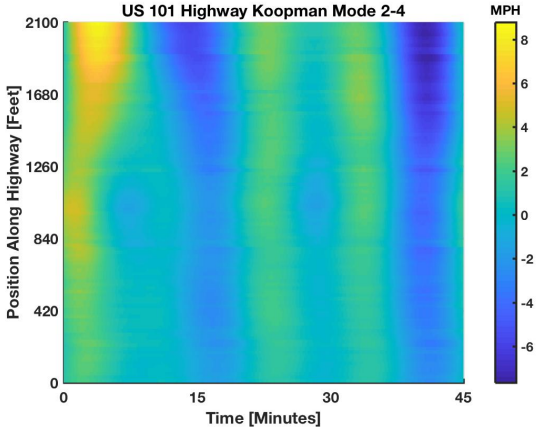

(c) Mode 2-4 Top View

Figure 4.5: Different Superpositions of Modes 2-4

of the highway (680ft-1280 ft).

The first three modes were dominant in the post ramp section of the highway however, the fourth mode seems to be more spatially extended over the entire section of highway. It has a peak in amplitude within the middle section of the highway (840ft-1260ft) and seems to display a slight increase in amplitude between the off-ramp and mid-ramp (2100ft-1260ft) and a decrease in amplitude between the mid-ramp and off-ramp (700ft-0ft). This is evidence of the pumping effect referred to in [68] and [48] however, there are other modes that better display this effect. Figure 4.6b better demonstrates the mid-

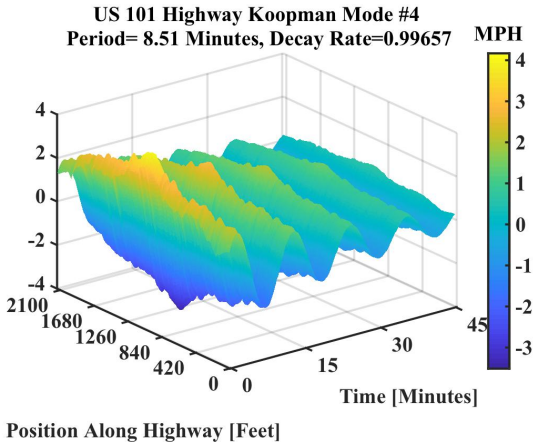

(a) Mode 4

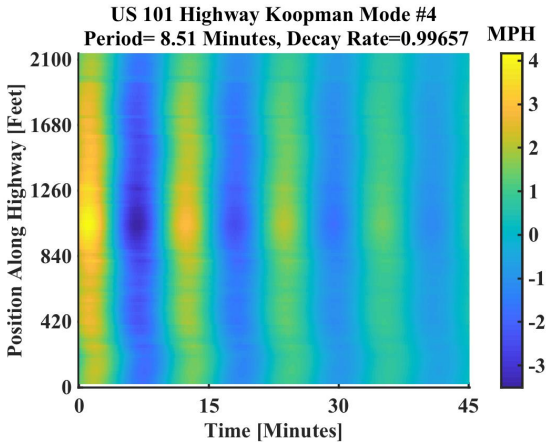

(b) Mode 4 Top

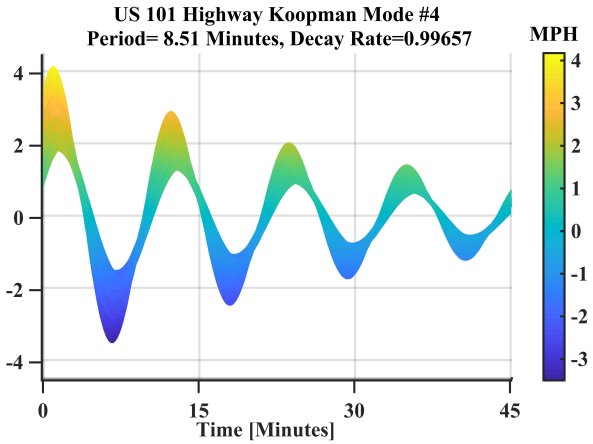

(c) Mode 4 Side

Figure 4.6: Mode 4

ramp peak in amplitude of mode 4. Lastly, the fourth mode is plotted on its side view to demonstrate the exponential temporal evolution of a mode.

Modes 5-7, shown below, are again spatially extended modes however, they do not decay in time like the fourth mode. The waves observed in modes 5-7 propagate through the highway with unperturbed speed or waveform. Their near-constant speed of propagation and stable spatial form indicates that these modes correspond to backward propagating jams.

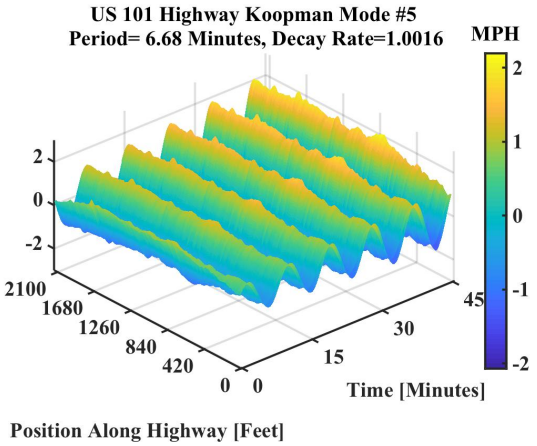

(a) Mode 5

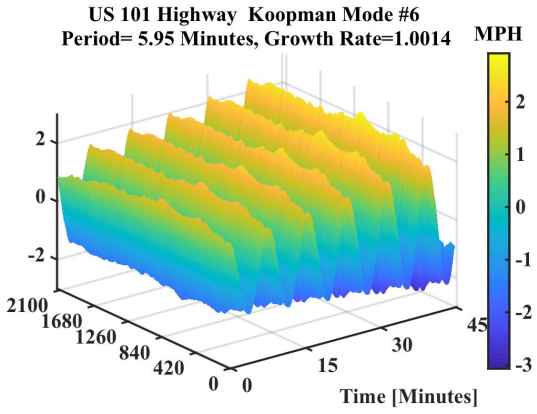

(b) Mode 6

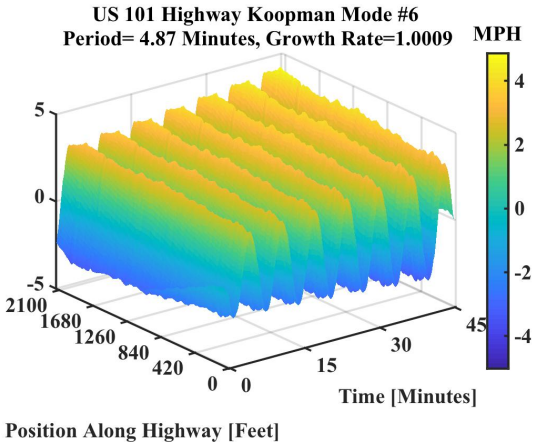

(c) Mode 7

Figure 4.7: Globally Extended Modes

Taking superpositions of the previously shown modes better shows which waves are phase-locked and those which are not. Figures 4.8a and 4.8b show how modes 4 and 5 and modes 6 and 7 superimpose constructively with each other. Lastly, figure 4.8c is a superposition of modes 4-7 which has both constructive and destructive regions.

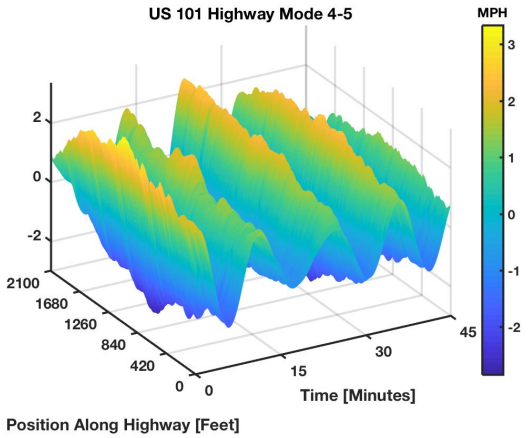

(a) Mode 4-5

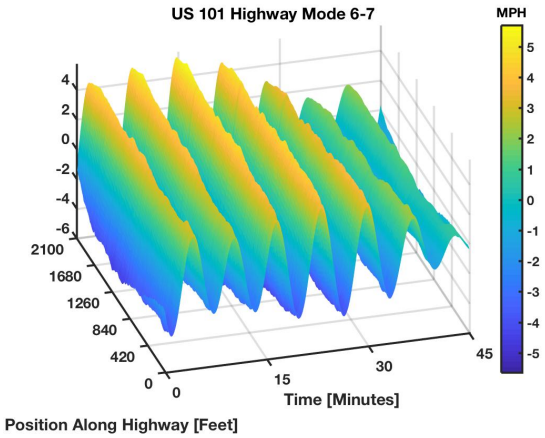

(b) Mode 6-7

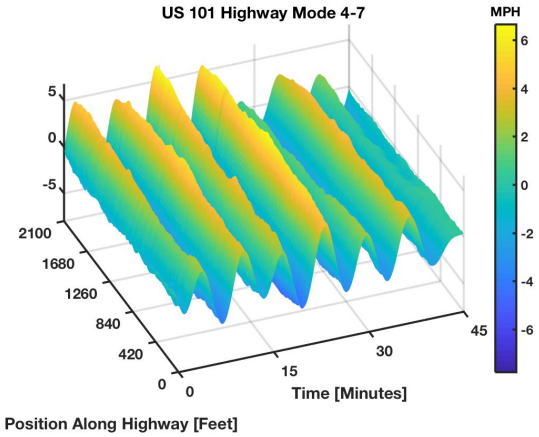

(c) Mode 4-7

Figure 4.8: Different Superpositions of Modes 4-7

Mode 8, shown below, exhibits a drop in wave amplitude when propagating past the off-ramp and again when passing the on-ramp. This effect is contrary to the proposed pumping effect where first an increase then a decrease in amplitude is expected. Evidence for the pumping effect is found in mode 9 where where a noticeable spike in amplitude is present between the ramps. Mode 10 is similar to modes 1-3 in that it is predominantly clustered in the post off-ramp section of the highway (1280ft-2100ft).

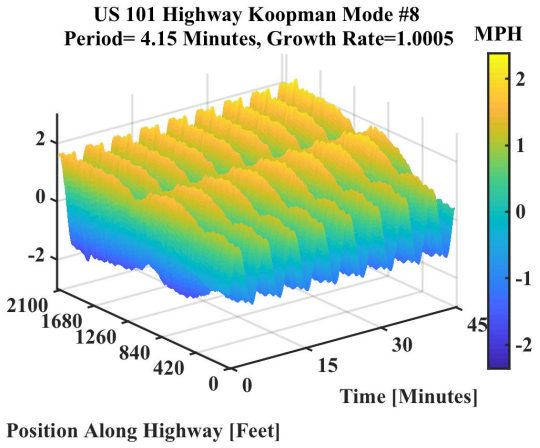

(a) Mode 8

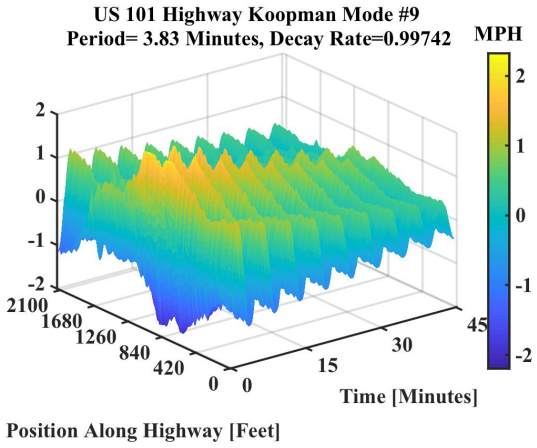

(b) Pumping Mode

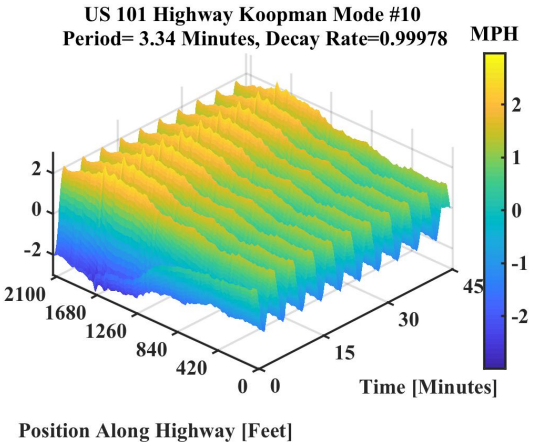

(c) Mode 10

Figure 4.9: Globally Extended Modes

4.2 Koopman Mode Analysis of NGSIM Lane Data

A similar mode analysis can be performed lane by lane in order to investigate any lane changing or lateral wave-like dynamics. After binning the trajectory density data lane by lane the data matrices are stacked into one tall matrix and decomposed simultaneously. The modes are then evolved in time and plotted side by side according to their lane. Since the ramp density is usually much lower than the highway density the ramp density has

been multiplied by 5 to better display the income and outflow. Our modes are now two-dimensional in space and therefore are best visualized as a movie in time. Plotted below in figure 4.10-4.18 are snapshots of these movie modes. The first mode, again, seems to correspond to the general transition from low to high density in the post-ramp section of the highway. This is best seen by comparing figures 4.10c-4.10f however, it is also apparent that not all the lanes are affected the same. In this first mode, the slow lanes (4 and 5), are heavily affected throughout the entire period of the mode and throughout the entire section of study. On the other hand, lane 1 farthest away from the ramp seems mostly unaffected in the on to mid-ramp section of the highway (0ft-1240ft). Lane 3 seems to experience a traveling jam which is best seen by comparing figures 4.10a-4.18. A laterally propagating pattern appears between figures 4.10f-4.10h, where the incoming on-ramp traffic is seen to propagate from the on-ramp over to lane 5 and then over to lane 4. This is intuitive and corresponds to the fact that oncoming traffic must merge into the highway from the ramp in order to continue traveling on the highway. Likewise, although a bit more elusive, it is possible to see in figure 4.10g and 4.10h a transition of vehicles from lane 3 to lane 5 and into the ramp section. This corresponds to the fewer set of vehicles that must transition into the off-ramp in order to exit the highway.

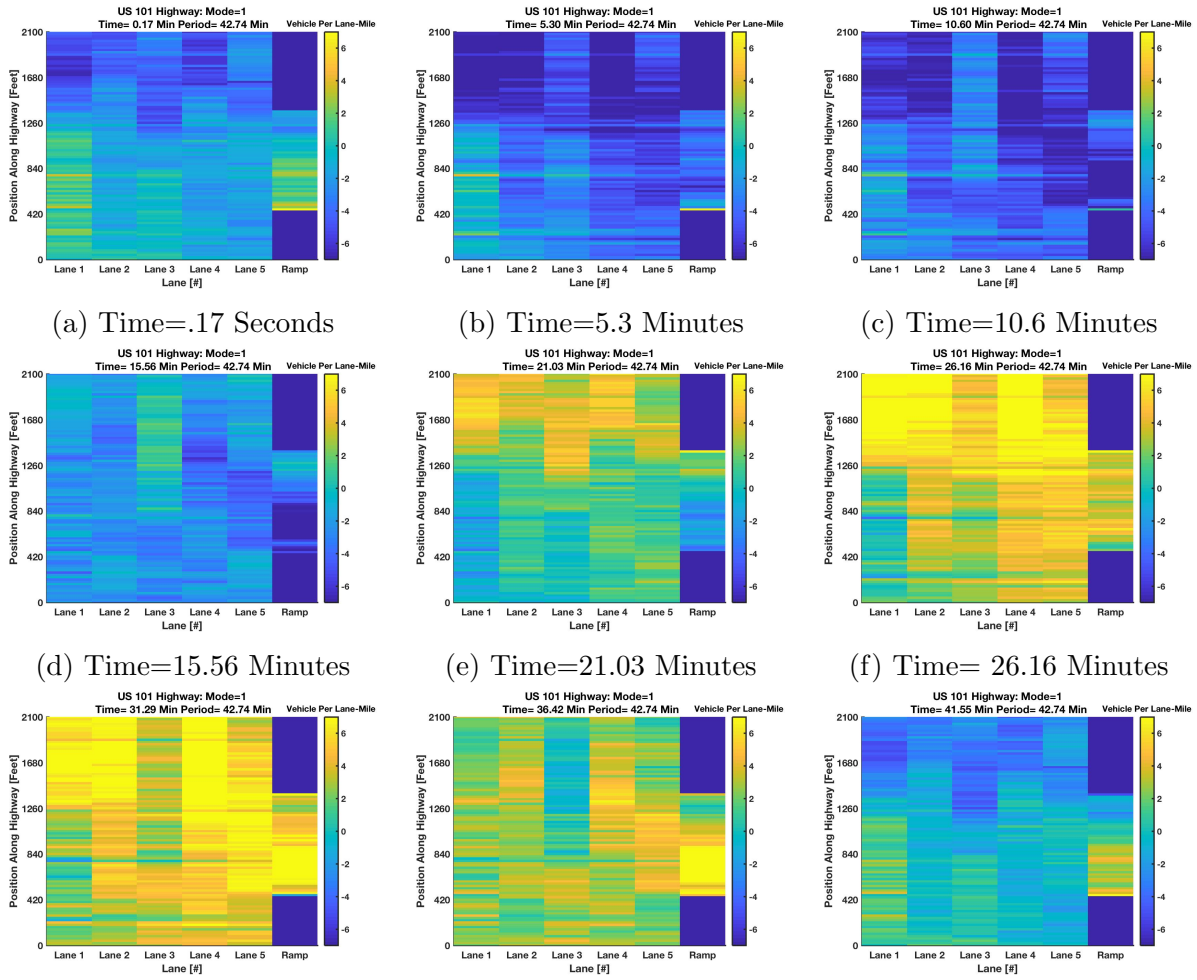

(a) Time=.17 Seconds (b) Time=5.3 Minutes (c) Time=10.6 Minutes

(d) Time=15.56 Minutes (e) Time=21.03 Minutes (f) Time= 26.16 Minutes

(g) Time=31.29 Minutes (h) Time=36.42 Minutes (i) Time= 41.55 Minutes

Figure 4.10: 1st Koopman Mode [Period=42.73 Minutes]

The next Koopman Mode, shown below, appears to be a half period harmonic of the first. Indeed, their spatiotemporal characteristics are similar in that there is an overall transition of low to high densities. Again, the lane changing behavior appears within this mode in the exact way as before. Figures 4.11b and 4.11g display how the merging vehicles lane change from lane 5 to lane 2 and how diverging vehicles lane change from lane 3 to lane 5. An interesting feature found in figures 4.11f-4.11h is evidence for how these lane changing maneuvers can be catalysts for backward traveling jams. For

example, in figure 4.11f there is an apparent lane changing of vehicles into lane 2 within the 1260ft-2100ft section. This lane changing maneuvering causes a jam to form and propagate backward all the way into the 840ft mark along lane 2 best seen in figures 4.11f-4.11h. Lastly, it is quite clear how the on-ramp densities seem to be out of phase with the highway densities. By this we mean that when densities appear to be high on the highway there is little to no inflow from the ramp and likewise there is an apparent inflow of traffic only when the density along the highway is low again. We believe this indicates how the inflow of merging traffic precedes the spike in highway density and likewise, a drop in density occurs when there are no more incoming vehicles.

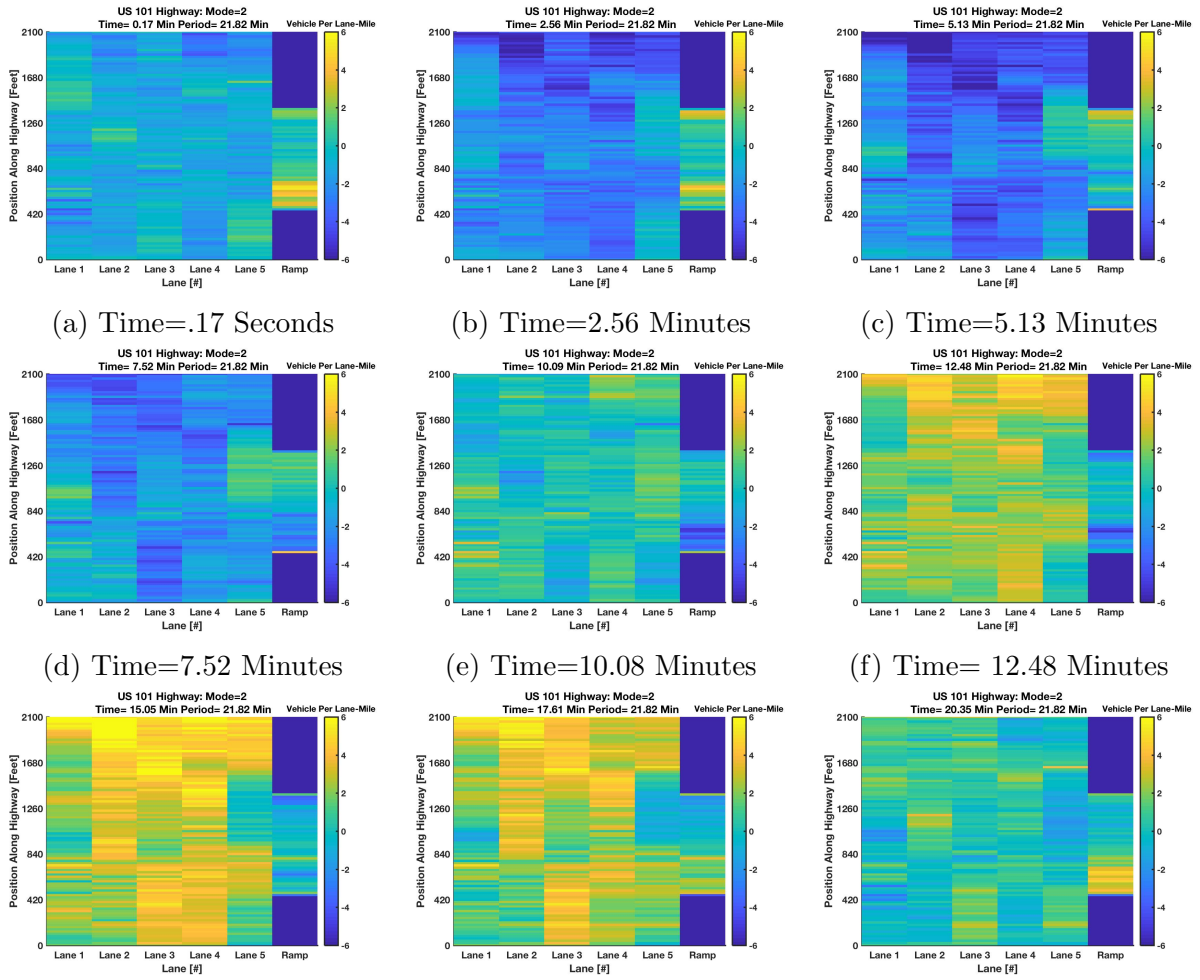

(a) Time=.17 Seconds

(b) Time=2.56 Minutes

(c) Time=5.13 Minutes

(d) Time=7.52 Minutes

(e) Time=10.08 Minutes

(f) Time= 12.48 Minutes

(g) Time=15.04 Minutes

(h) Time=17.61 Minutes

(i) Time= 20.35 Minutes

Figure 4.11: 2nd Koopman Mode [Period=21.82 Minutes]

A distinctive feature of the third mode is the activity within the on/off-ramp section best seen in figures 4.12b-4.12c. Figure 4.12b shows a cluster of vehicles at the off-ramp location exiting the highway which continues for the next few minutes until the highway exiting subdues and highway entering begins in figure 4.12d. This inflow remains until about figure 4.12f at which point lane changing into lanes 5 and 4 occurs near the 600ft and 850 ft mark. However, the clusters in lanes 5 and 4 also cause a backward propagating traffic jam to form in those lanes, which is best seen in figures 4.12f and

4.12g. This downstream traveling cluster of vehicles continues until about the 1800 ft mark where lane changing into lanes 3 and 2 occurs, best seen in figures 4.12f and 4.12g. Similarly, these lane changing maneuvers create a backward propagating jam in lane 2, figures 4.12h-4.12i. It is interesting to note how the incoming traffic begins to diminish starting in figure 4.12f and continues to do so until reaching a minimum at figure 4.12i. This drop in incoming vehicles persists into figures4.12a and 4.12b and is amplified in figure 4.12c when highway exiting is at its peak again. This is similar to the previous mode in where we observed a noticeable phase difference between the ramp and highway densities.

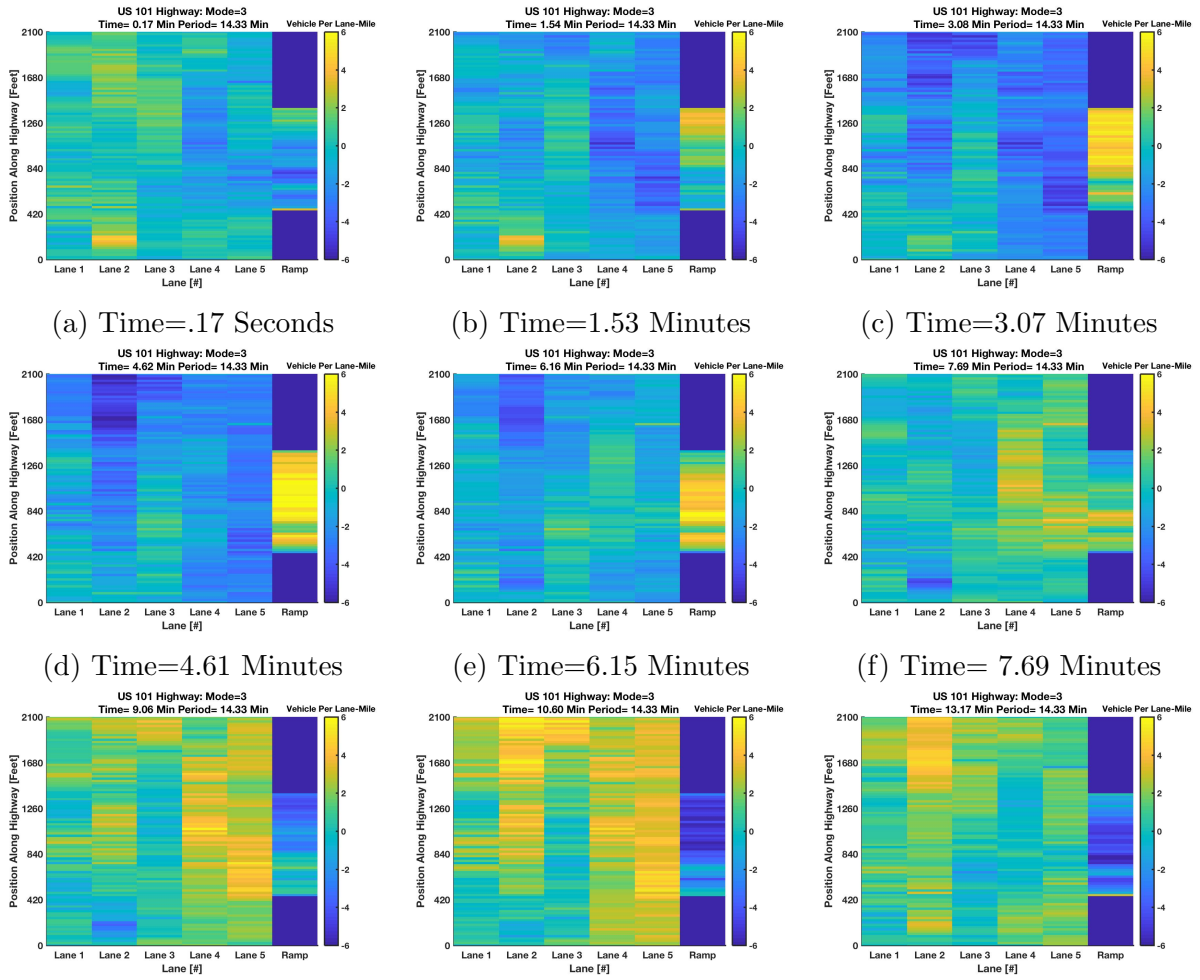

(a) Time=.17 Seconds (b) Time=1.53 Minutes (c) Time=3.07 Minutes

(d) Time=4.61 Minutes (e) Time=6.15 Minutes (f) Time= 7.69 Minutes

(g) Time=9.06 Minutes (h) Time=10.6 Minutes (i) Time= 13.16 Minutes

Figure 4.12: 3rd Koopman Mode [Period=14.33 Minutes]

The fourth mode contains a backward traveling jam that eventually displaces laterally and continues to propagate in the adjacent lanes. The process begins in figure 4.13i and 4.13a with the apparent inflow of merging traffic from the on-ramp which propagates into lanes 5 and 4 shown in figures 4.13b and 4.13c. The lane changing causes a traveling jam in lane 2 which propagates backward until momentarily halting at the 1000ft mark, shown in figure 4.13e, and continuing in the adjacent lanes 3 and 2 shown in figures 4.13f-4.13h. Overall, the fourth mode seems to capture the dynamics of traveling traffic

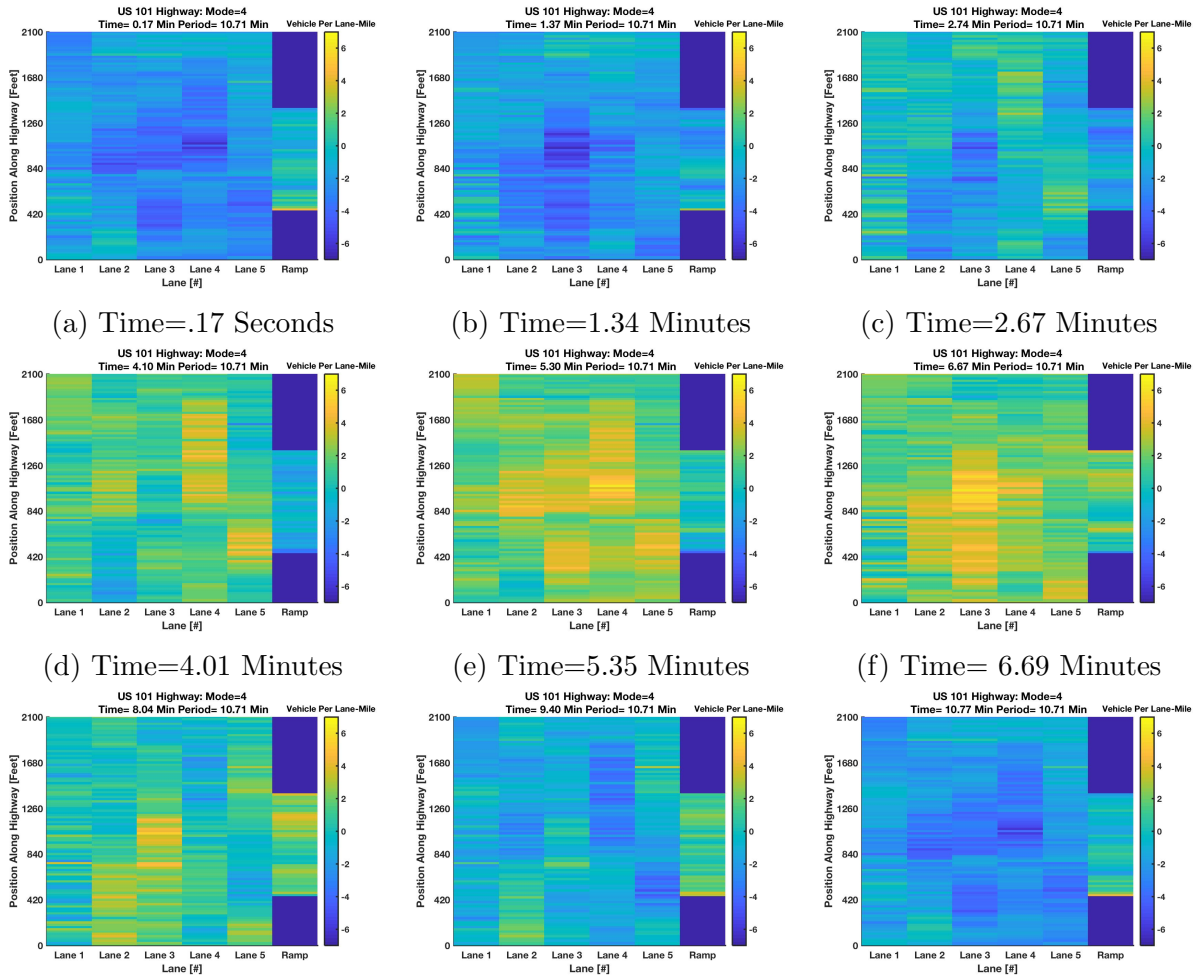

(a) Time=.17 Seconds (b) Time=1.34 Minutes (c) Time=2.67 Minutes

(d) Time=4.01 Minutes (e) Time=5.35 Minutes (f) Time= 6.69 Minutes

(g) Time=8.02 Minutes (h) Time=9.36 Minutes (i) Time= 10.7 Minutes

Figure 4.13: 4th Koopman Mode [Period=10.7 Minutes]

jam waves that have combined longitudinal and lateral travel. Traffic jams appearing in adjacent lanes have commonly been observed during empirical studies**??**.

Mode 5 is similar to 4 in that it travels longitudinally and laterally over to adjacent lanes when passing the ramp section. Therefore we, skip to Mode 6 shown below in figure 4.14. Figures 4.14c-4.14e illustrate a backward propagating jam in lanes 1 and 2 make its way into our field of observation. The jam stops momentarily near the 840 ft mark, moves over laterally into lanes 2 and 3 and then continues propagating down lanes 2 and 1, best seen in figures 4.14f-4.14h.

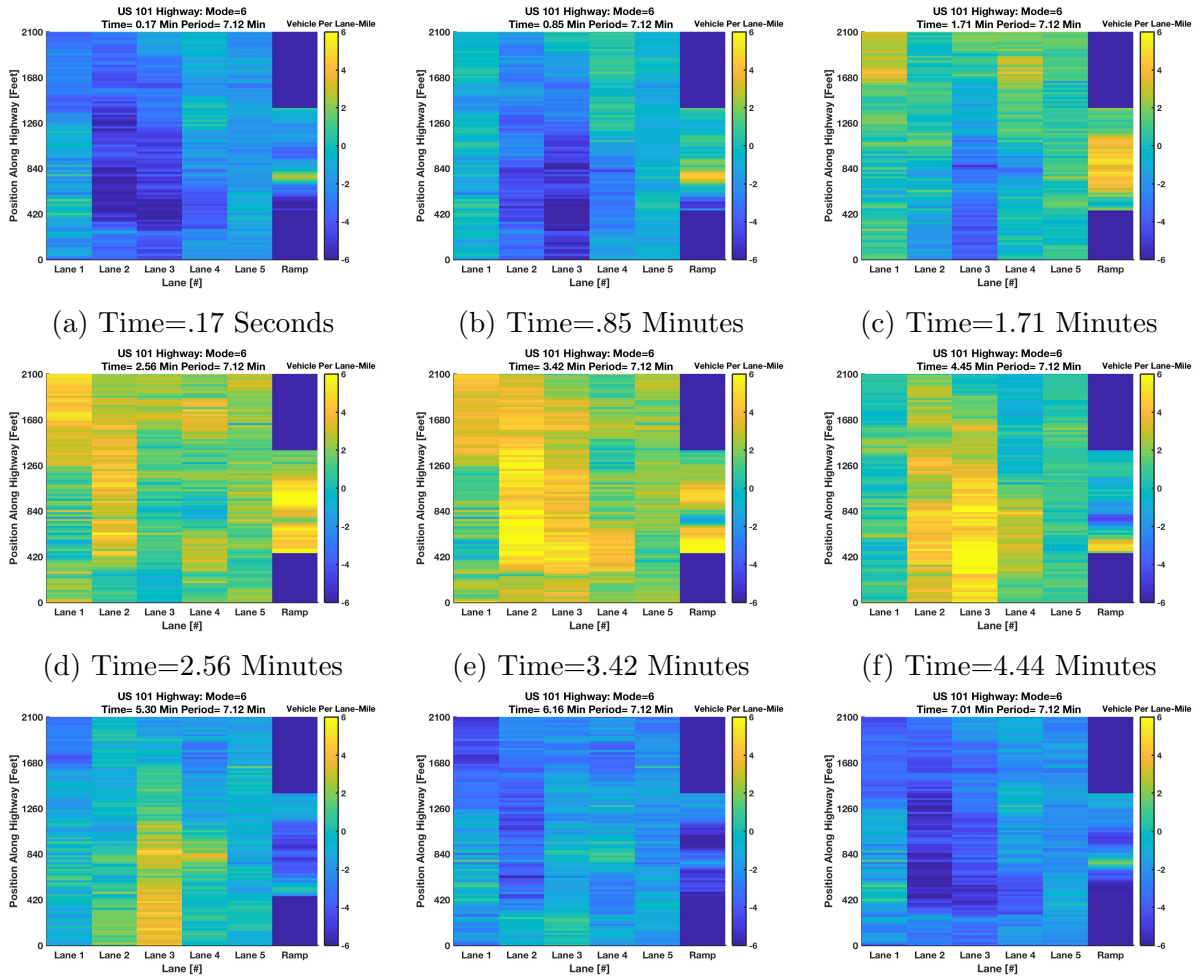

(a) Time=.17 Seconds (b) Time=.85 Minutes (c) Time=1.71 Minutes

(d) Time=2.56 Minutes (e) Time=3.42 Minutes (f) Time=4.44 Minutes

(g) Time=5.3 Minutes (h) Time=6.15 Minutes (i) Time= 7.01 Minutes

Figure 4.14: 6th Koopman Mode [Period=7.12 Minutes]

Mode 7 is shown below in figure 4.15 and corresponds to a heavy highway wide traffic jam that propagates through all lanes. It is interesting to see how the jam not only propagates backward but also laterally towards the off-ramp, which gives it that apparent north-west to south-east direction of travel. This mode can be seen to be affecting all the lanes in the same way. The wave in this mode travels past the on/off-ramps completely unperturbed and very well corresponds the modes found earlier in figure 4.9

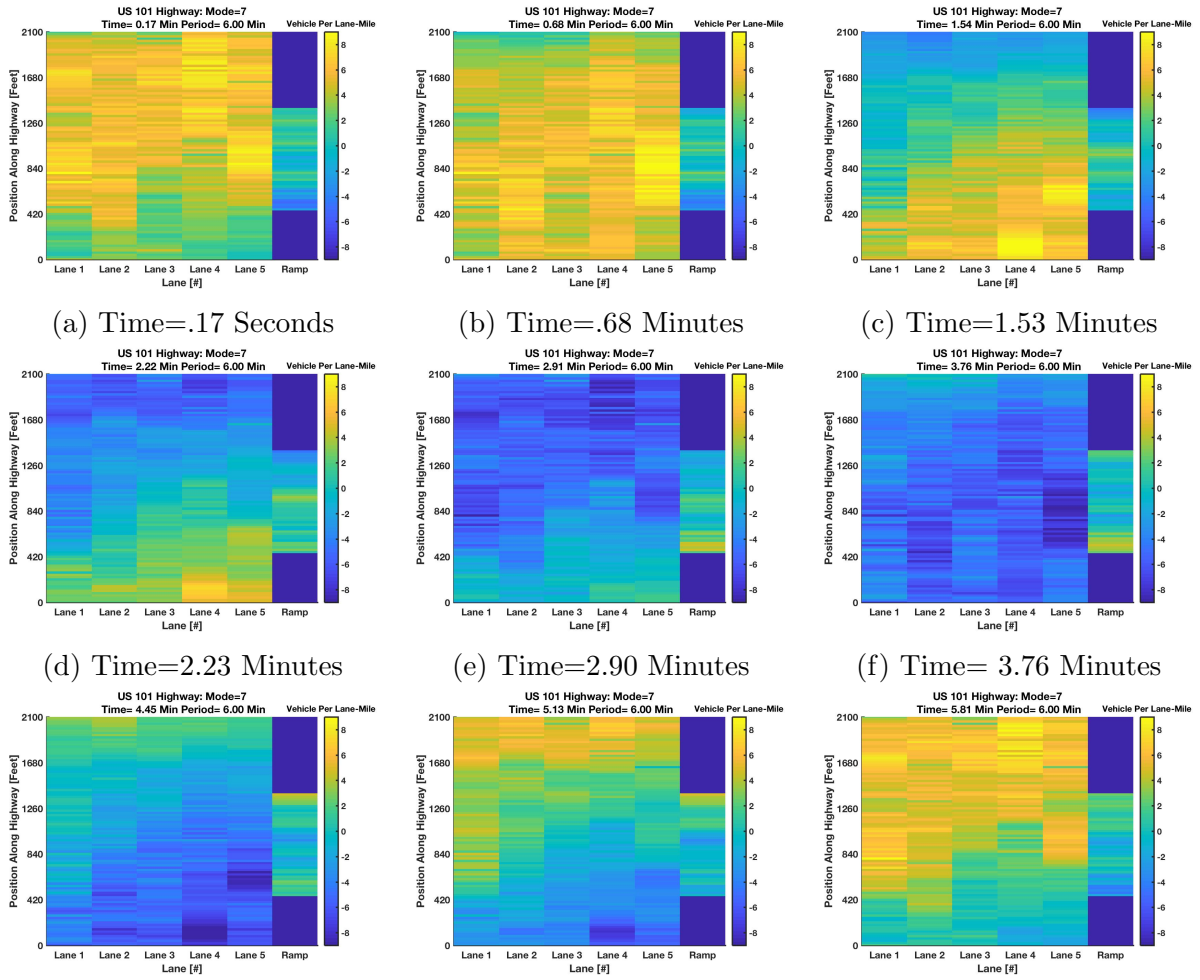

(a) Time=.17 Seconds (b) Time=.68 Minutes (c) Time=1.53 Minutes

(d) Time=2.23 Minutes (e) Time=2.90 Minutes (f) Time= 3.76 Minutes

(g) Time=4.46 Minutes (h) Time=5.13 Minutes (i) Time= 5.8 Minutes

Figure 4.15: 7th Koopman Mode [Period=6 Minutes]

Mode 8 seems to capture the drivers exiting the highway when faced with near stopped traffic conditions. This phenomenon can best be seen by starting in figure 4.16d where traffic jams begin to form near the post-ramp section in lanes 1, 2 and 3 and then form in lanes 4 and 5 in figure 4.16e. By figure 4.16f the jams have propagated past the off-ramp into the mid-section. Figures 4.15 and 4.16 show how the jams in lanes 1-3 have propagated by, however, the jams in lanes 4 and 5 seem to stop and form a localized cluster near the 840 ft mark. The clusters in lanes 4 and 5 cause a movement of vehicles

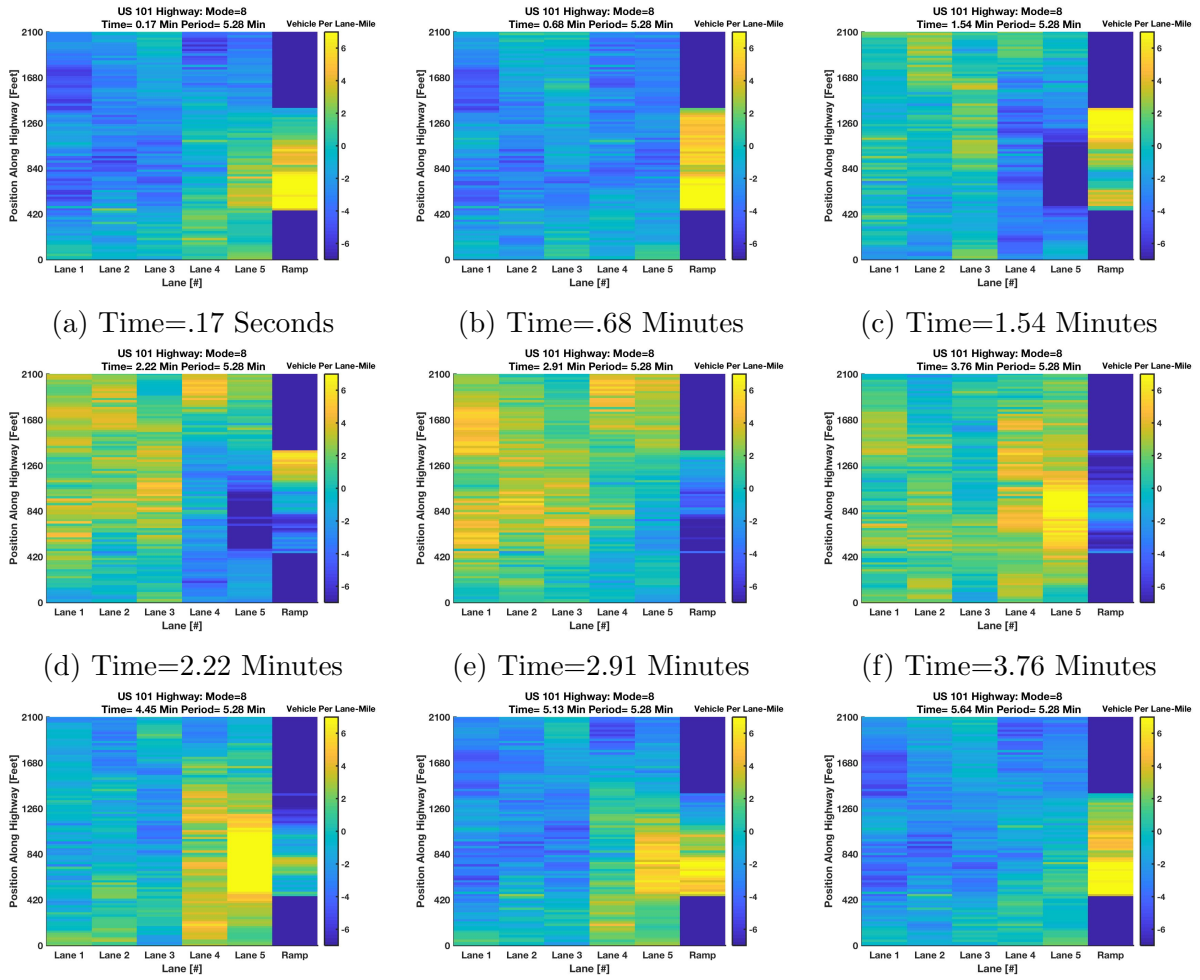

(a) Time=.17 Seconds (b) Time=.68 Minutes (c) Time=1.54 Minutes

(d) Time=2.22 Minutes (e) Time=2.91 Minutes (f) Time=3.76 Minutes

(g) Time=4.45 Minutes (h) Time=5.13 Minutes (i) Time=5.64 Minutes

Figure 4.16: 8th Koopman Mode [Period=5.27 Minutes]

into the ramp best seen in figure 4.16i, after which the vehicles continue down the ramp to exit, best seen in figures 4.16a-4.16b.

An interesting feature found in the backward propagating modes is the zig-zag motion they tend to exhibit when passing by the mid-ramp section. Mode 10, shown below, in figure 4.17 very well displays a lateral the displacement of a traveling jam from the slow-moving lanes into the fast-moving lanes. The wave propagates shortly, until jumping back into the slow moving lanes. This is best seen by starting in figures 4.17g and 4.17h where jams begin to form within the 1260ft-2100ft mark in lanes 3-5. By figure 4.17i those

jams have propagated laterally over to now occupy lanes 1-4. Next, in figures 4.17a and 4.17b the jams in lanes 1 and 2 continue to propagate but the lane 3 jam seems to halt and cluster around the 0-420 ft mark. This causes a cluster of vehicles to again occupy lanes 3-5 best seen in figure 4.17c. This zig-zag like effect could well be responsible for the change in speeds of propagation observed earlier in figures 4.5b-4.5c.

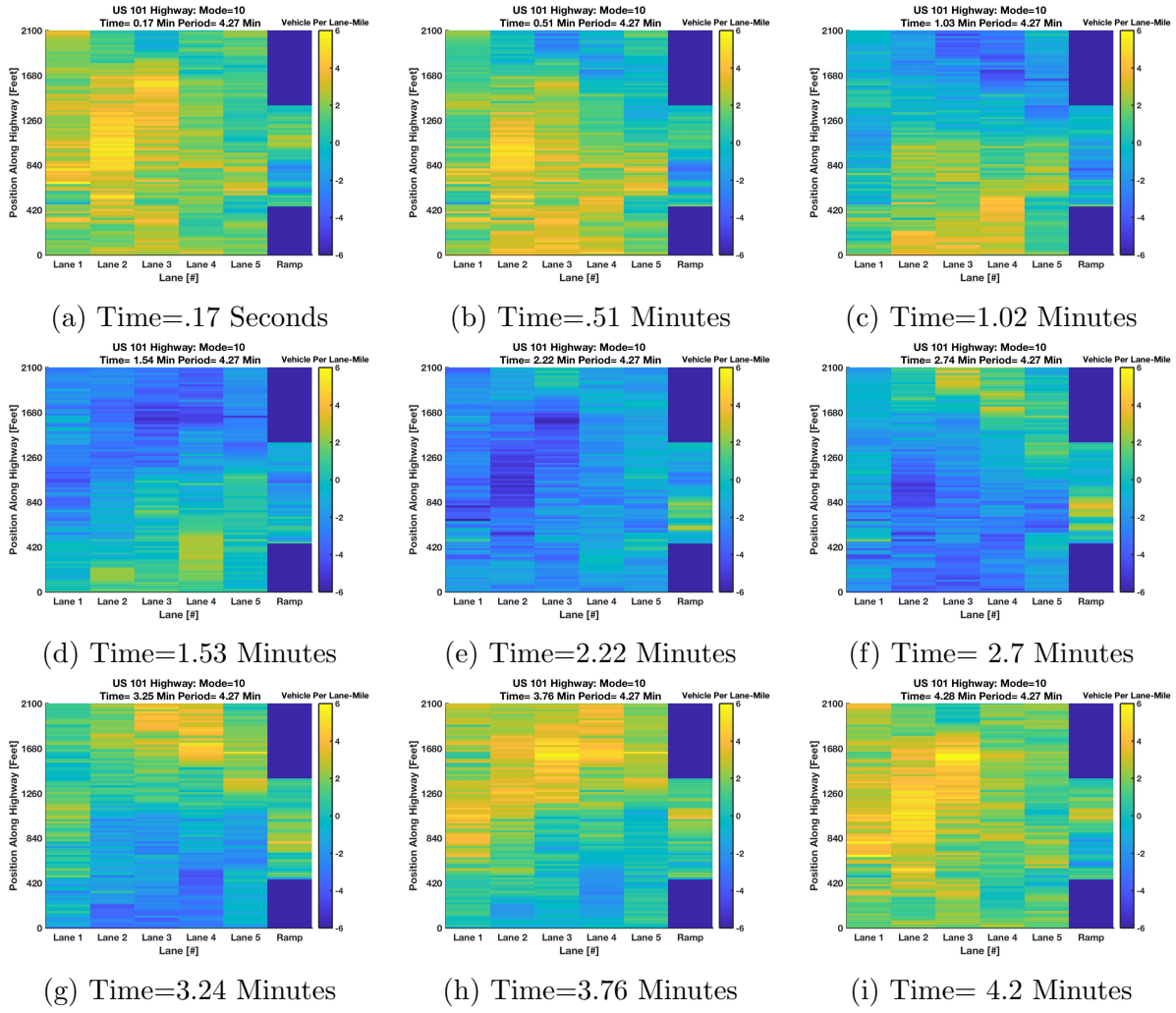

(a) Time=.17 Seconds

(b) Time=.51 Minutes

(c) Time=1.02 Minutes

(d) Time=1.53 Minutes

(e) Time=2.22 Minutes

(f) Time= 2.7 Minutes

(g) Time=3.24 Minutes

(h) Time=3.76 Minutes

(i) Time= 4.2 Minutes

Figure 4.17: 10th Koopman Mode [Period=4.27 Minutes]

Next we plot the 14th mode which is much like the 7th mode in that we see backward traveling traffic jams that span the entire highway. The interesting fact here is that the

14th mode has a period of 3.1 minutes which is close to exactly half that of the 7th mode which has a period of 6 minutes. Figure 4.18 illustrates the highway wide wave-like dynamics of mode 14.

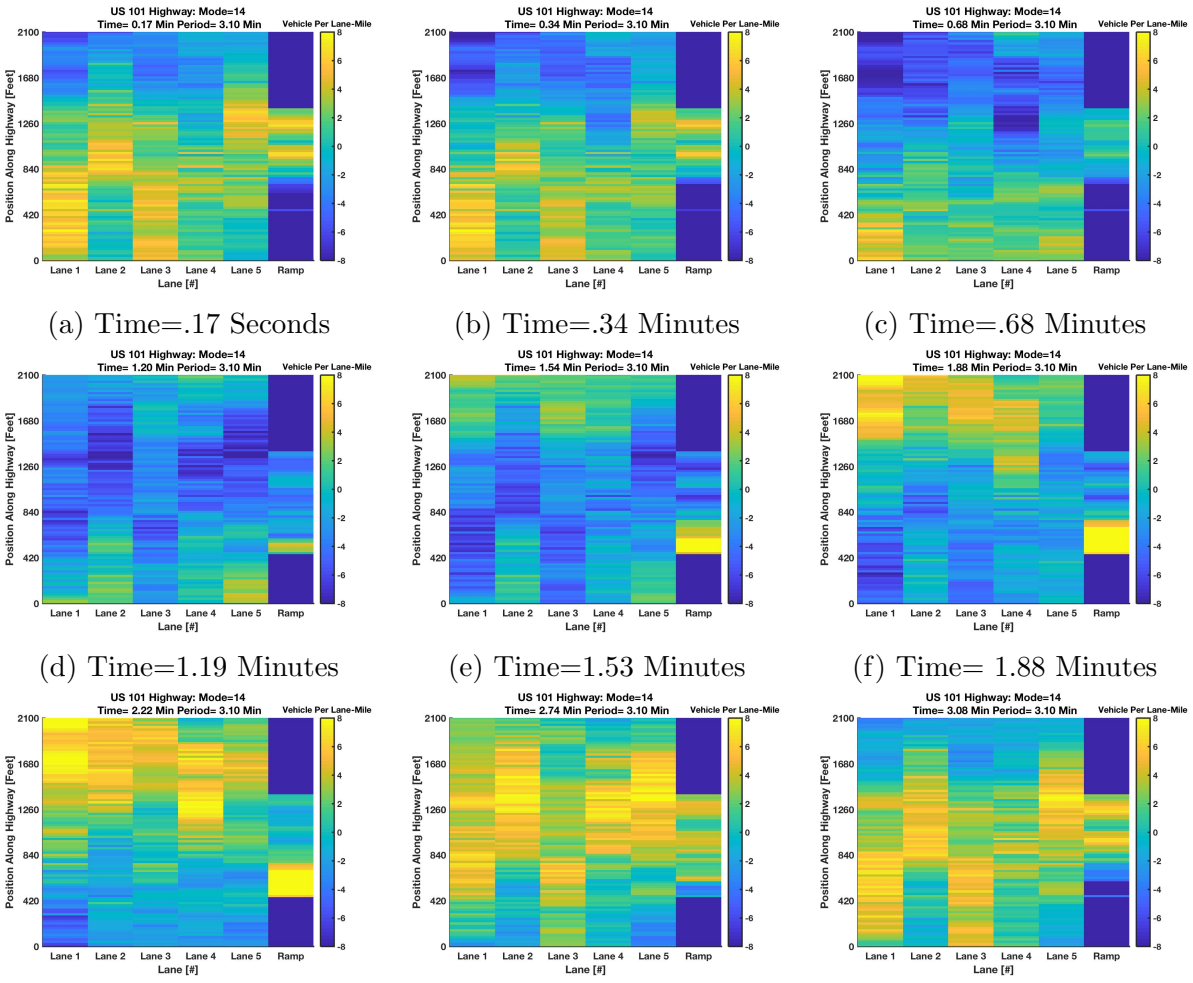

(a) Time=.17 Seconds

(b) Time=.34 Minutes

(c) Time=.68 Minutes

(d) Time=1.19 Minutes

(e) Time=1.53 Minutes

(f) Time= 1.88 Minutes

(g) Time=2.23 Minutes

(h) Time=2.73 Minutes

(i) Time= 3.07 Minutes

Figure 4.18: 14th Koopman Mode [Period=3.1 Minutes]

By analyzing our modes we seek to find evidence for or against past research findings. It is mentioned in [68] how previous research has aimed at determining the effects of bottlenecks on the amplitudes of traffic waves. The works of [48] find that on-ramps do have an effect on the amplitudes of oscillation through what is called the "pumping"

effect. Specifically, it was shown how amplitudes of oscillation decrease when propagating past on-ramps. Similarly, it assumed that off-ramps would would cause an increase in the amplitude of oscillation but no validation for this is given in[48][68]. We find evidence of such phenomenon in mode 9 and evidence for the exact opposite in mode eight and ten. Figures 4.9a and 4.9c show a drop in amplitude when passing from the off-ramp to the mid-ramp section and another drop when passing into the on-ramp section. Additionally, the works of [83] have shown a relation between the periods of oscillation and the amplitudes, in where they state how long periods are usually accompanied by large amplitudes and short period oscillations usually have low amplitudes. We find evidence for this trend, shown below in figure 4.19a where the max amplitude of each mode is plotted against its period. Similarly, the car-following model proposed in [84] indicates how low frequency oscillations should grow in amplitude as they propagate through traffic and that high frequency oscillations will decay in time. Looking back to figures 4.3-4.9, one can see how high period (low-frequency) modes tend to have growth rates and those with higher frequencies have decay rates. Figure 4.19b below is evidence for such a phenomenon where the growth/decay rates have been plotted against the period.

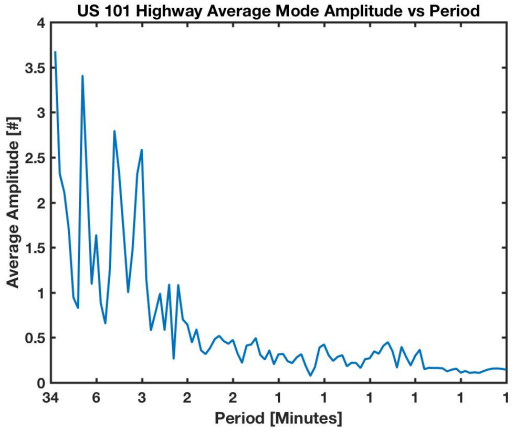

(a) US 101 Highway: Average Amplitude vs Period

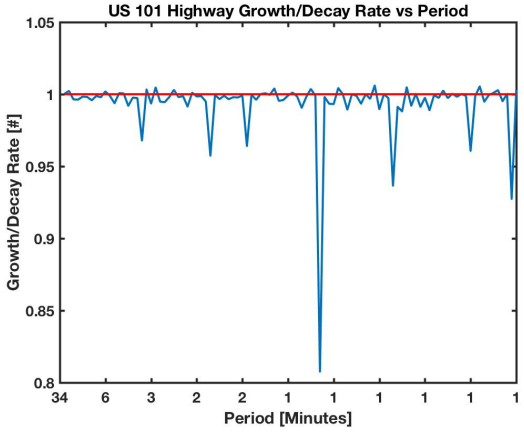

(b) US 101 Highway: Growth/Decay Rate vs Period

4.3 Reconstruction of NGSIM Data

We now apply 5 delays for the US 101 and US 80 5pm highways, 3 delays for the US 80 4pm highway and then reconstruct our data by evolving the all the modes for an equivalent time of forty-five, fifteen and thirty minutes. Figure 4.20 below shows the KMD reconstruction of the US 101 and US 80 velocity data sets. Plots of the density and flow reconstruction, for both highways, can be referenced in the appendix.

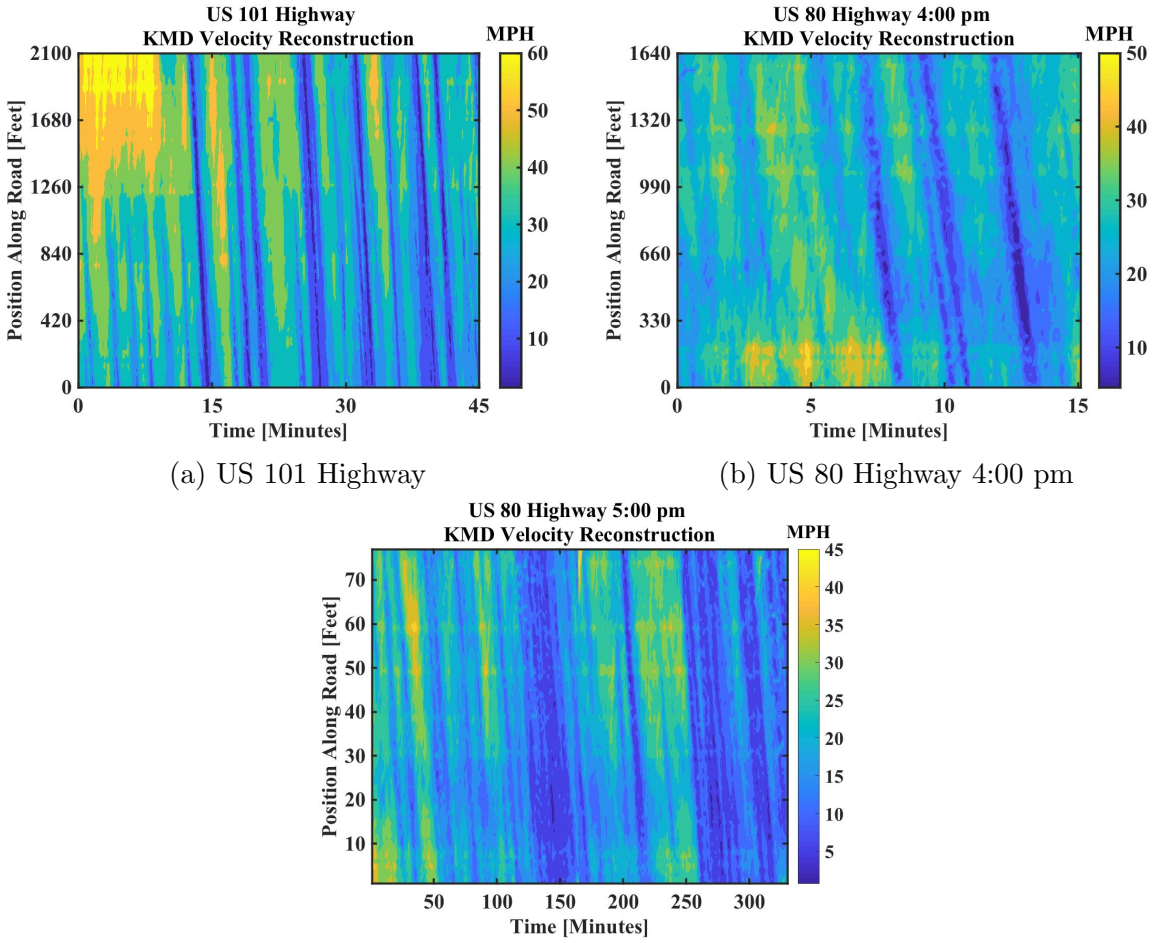

(a) US 101 Highway

(b) US 80 Highway 4:00 pm

(c) US 80 Highway 5:00 pm

Figure 4.20: KMD Velocity Reconstruction

We emphasize how our method of reconstructing spatiotemporal data differs from traditional methods utilized within the traffic physics community. Traditional methods typically utilize statistics or nonlinear filtering techniques together with traffic flow models to reconstruct observed data [47][77][78]. The KMD differs in that it does not filter or fit data in any way. Rather, the KMD represents the dynamics of a nonlinear system in terms of the spectrum of a linear, infinite-dimensional, operator. The eigenvalues and eigenfunctions of the Koopman operator capture key properties of the dynamics and are inherent to the system. The Koopman modes capture spatiotemporal patterns that depend on the modality of observation and offer a platform for reconstructing and forecasting observed quantities. The KMD accomplishes this without the need of a dynamic model, parameter tuning or smoothing of data.

4.4 Error Analysis

While the accuracy of the KMD's reconstruction is evident by simple visual comparison of figures 3.2 and 4.20, there are few discrepancies between the real and reconstructed data. A percent error matrix was calculated according to the formula shown below. Next, the total average error (TAE) was calculated by averaging the elements of the error matrix over the space-time domain. Figure 4.21 shown below demonstrates a contour of the percent error matrix for the US 101 highway data sets.

$$Error(i,j) = \frac{|X(i,j) - X(i,j)_{DMD}|}{|X(i,j)|} \tag{4.5}$$

$$\text{Total Average Error} = mean_t(mean_x(Error)) \tag{4.6}$$

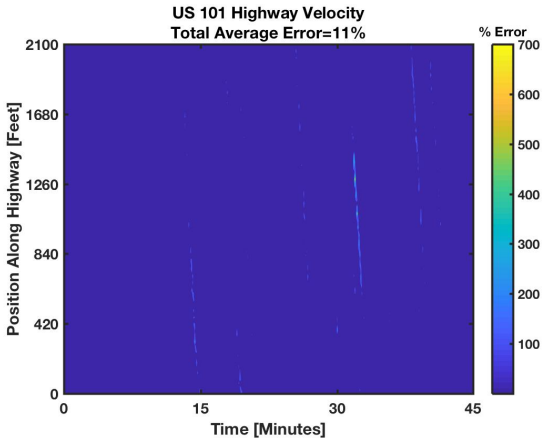

(a) US 101 Error:12%

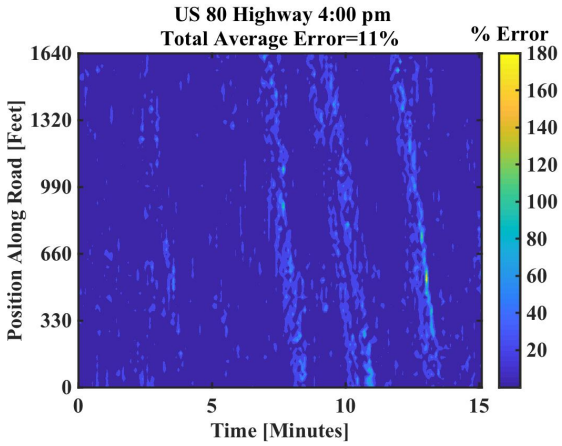

(b) US 80 4:00pm Error:11%

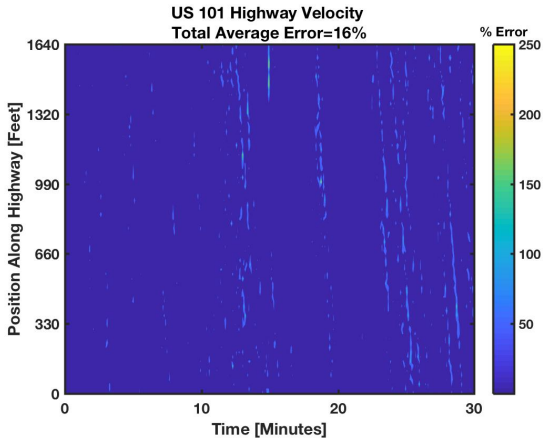

(c) US 80 5:00pm Error:16%

Figure 4.21: KMD Velocity Reconstruction Average Error

The greatest sources of error in Figures 4.21a-4.21c, despite being large, all occurred in a very localized fashion about the traffic jams. This is beneficial for the purpose of traffic forecast and reconstruction because localized error does not distort global structure by much. Therefore, accurate reconstruction of global spatiotemporal patterns are still obtained, which is evident in the relatively low TAE of about 12%-19% and the strong visual similarities between the original and reconstructed data. The following table summarizes our TAE in reconstruction. Plots of the percent error matrix for the US 80 highway can be referenced in the appendix.

	US 101 Highway	US 80 Highway 4:00 PM	US 80 Highway 5:00 PM
Velocity	11%	11%	16%
Density	17%	18%	19%
Flow	19%	18%	19%

Table 4.1: Table of Total Average Error

A potential source of error could be due to the residual term in equation 8. This would imply that we have not sampled enough of the state space to obtain a sufficiently rich basis of eigenfunctions. It may also be that the dynamics are so highly nonlinear that theoretically, an infinite amount of eigenfunctions are needed for a perfect reconstruction. It may also be that our system contains continuous spectrum in addition to its discrete spectrum. Noise or any systematic error introduced by our construction of macroscopic quantities could also be contributing to the error. A possible cause for the large errors near the traffic jams is the fact that sharp transitions in the state cannot be captured by a single Koopman mode but rather a superposition of several phase-locked modes. Therefore, numerical errors in the frequency of oscillations will cause modes to be slightly out of phase. Furthermore, this phase difference error or any other numerical errors in growing modes will increase exponentially in time, due to the nature of equation 2.11. The number of delays to take for an accurate reconstruction is not exactly specified by any theorem therefore, we also explore how reconstruction error depends on the number of delays. We do this by reconstructing the data under various delays and recording our error each reconstruction. Applying this process to the NGSIM data sets yields figure 4.22 shown below. Figures 4.22a-4.22c all demonstrate a huge (23 orders of magnitude) spike in error corresponding to the number of delays that yield a near square matrix (Not visible in Figure 4.22a). Taking delays beyond that point we obtain stable error variation

with increasing delays. More importantly, we can see that the method of time-delays can yield better results than just decomposing the original data. In all cases, we observe a drop in the TAE once the delay embedding yields a square data matrix. Moreover, this error remains stable (less than 1% deviation) for increasing delays. Therefore, in this work, we take sufficient delays so that our new embedded data matrix is at least tall.

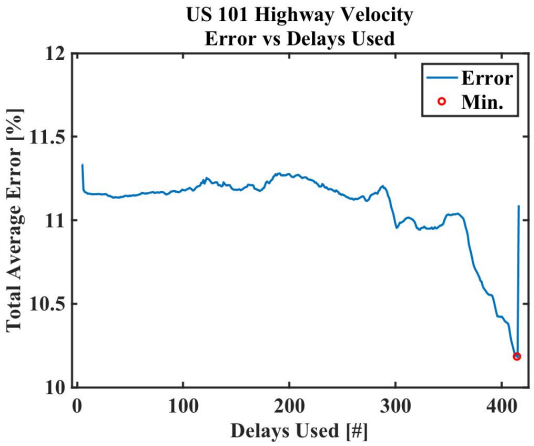

(a) US 101 Highway

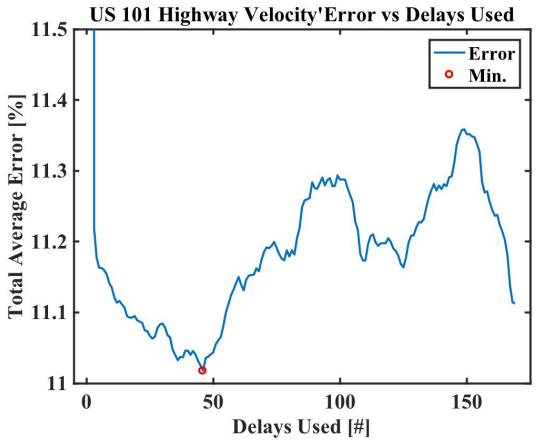

(b) US 80 Highway 4:00 pm

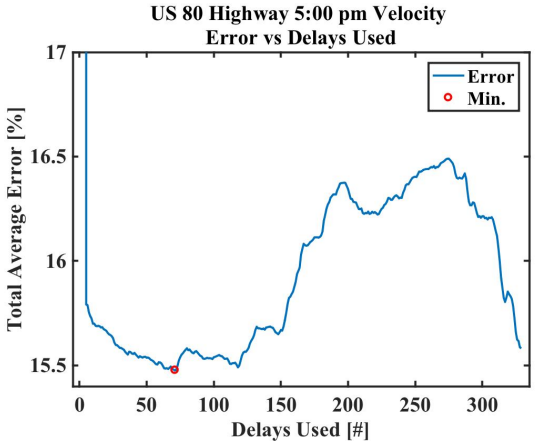

(c) US 80 Highway 5:00 pm

Figure 4.22: Reconstruction Error vs Delays Used

Additionally, we also investigate the minimum number of modes needed for an accurate reconstruction under 7 delays for US 101 and US 80 5pm and 4 for US 80 4pm. Now, for every mode obtained there is a corresponding singular value resulting from the SVD

decomposition required by the DMD algorithm. We use these singular values to sort or rank the modes and then reconstruct our data with only one mode and increasing until we have used all of the modes. Recording the error along the way yields figure4.23 seen below, wherein all three cases we see that the most accurate reconstruction is obtained by using less than the total number of modes available. This indicates that not all of the Koopman modes obtained are dynamically important and some may correspond to noise or numerical errors.

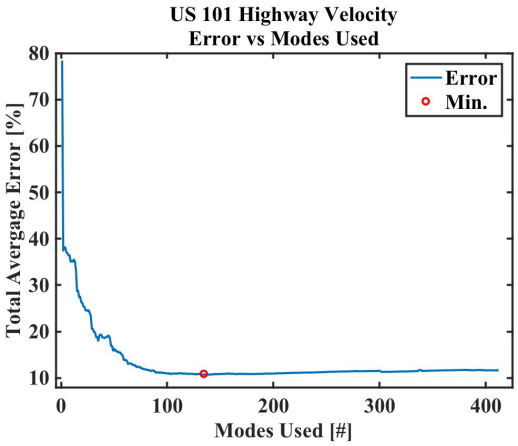

(a) US 101 Highway

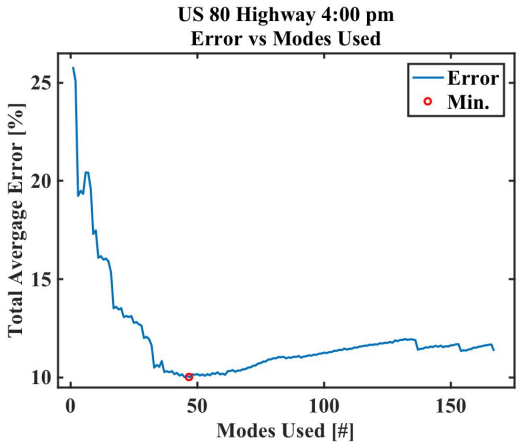

(b) US 80 Highway 4:00 pm

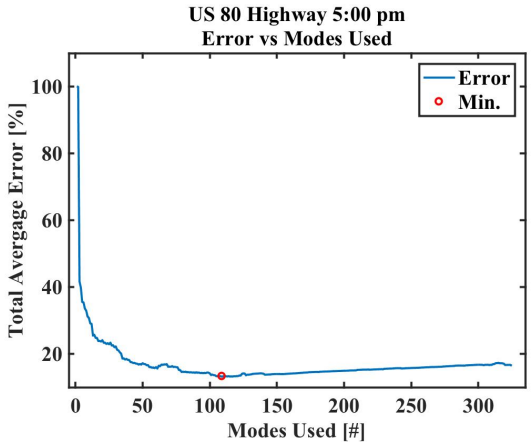

(c) US 80 Highway 5:00 pm

Figure 4.23: Reconstruction Error vs Modes Used

Chapter 5

Forecasting of Traffic

The accurate forecasting of traffic is an indispensable part of any intelligent transportation system (ITS) however, this task has proven to be an elusive and challenging problem [82][85][86]. In this work, two of the ten proposed research directions of [82] are addressed. The first is a call for the development of responsive algorithms and prediction schemes. Transportation agencies require forecasts that are robust to the short and long-term changes in traffic conditions. Most of the time these changes in the system are unknown and unexpected like adverse weather conditions or accidents. This combination of recurring and not-so recurring events lead to a complex system and increase the difficulty of accurately forecasting. This unpredictable switching of dynamics has lead to much research into developing multi-regime models. These models have been extended to include weather and accidents but with added complexity and parameters [85] [86]. The second direction of research is the call for a generalized approach to identifying spatiotemporal patterns in traffic. It is argued how the knowledge of spatiotemporal patterns can lead to improved predictability of certain forecasting schemes. For example, identifying spatiotemporal patterns can lead to improved ramp-metering times that dampen oscillations as they propagate by [62]. The issue of identifying and analyzing spatiotemporal patterns from data has already been addressed in section 4. In this section a data-driven method for accurately forecasting short and long-term traffic dynamics is presented.

5.1 Forecasting of NGSIM Data

We now prescribe a method for forecasting macroscopic traffic states by utilizing a subset of s data vectors (sampling window) to predict the next p data vectors (prediction window). We first illustrate our procedure by applying it to the NGSIM data and then test our method for a week and month-long PeMS data set. Our forecasting scheme involves choosing a sampling and predicting window (s, p), which dictates how much past data we will use and how far into the future we will forecast. First, a KMD of our sampling window is obtained and the modes are evolved, according to equation (2.11), for $s + p$ time steps. We then slide our window forward one time step and repeat the procedure. Figure 5.1 below illustrates how the first three minutes of the NGSIM 101 Highway data can be used to predict the next two minutes.

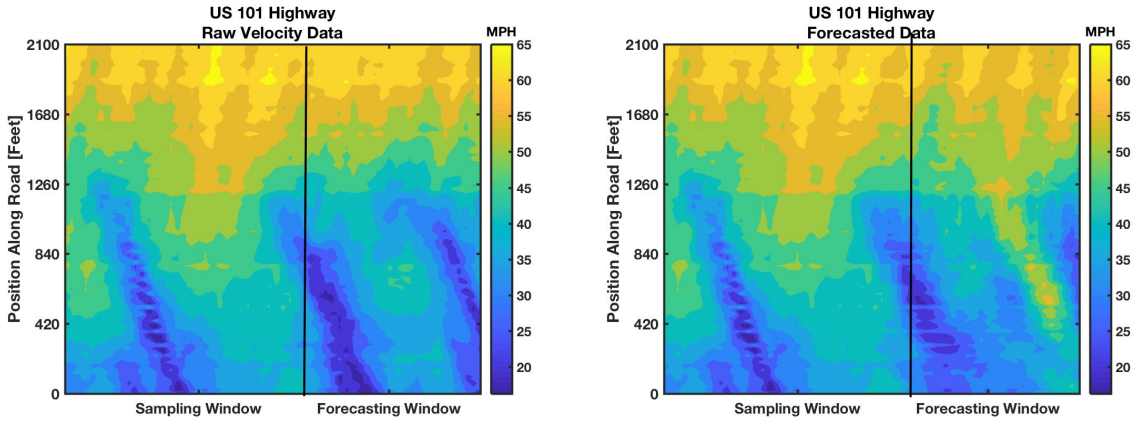

(a) Raw Data (b) Forecasted Data

Figure 5.1: US 101 Highway Velocity Data

Computing the error over the prediction window leads to the plot below in figure 5.2. The greatest source of error is in the forecasted regime and once again near or along the traffic jams.

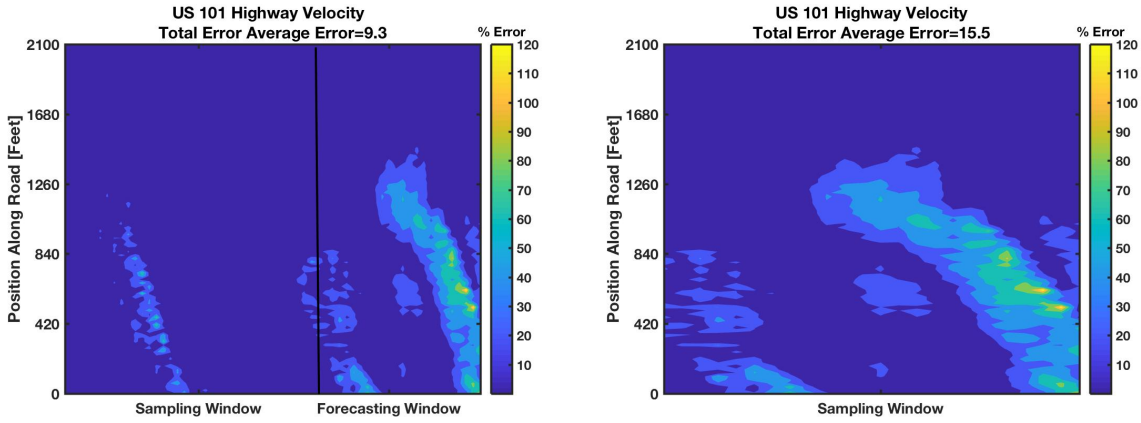

(a) Error in Sampling+Forecast (b) Error in Forecast

Figure 5.2: US 101 Highway Forecast Error

By sliding our window we are able to draw forecasts at every time step along the way and for every step we can use equation (4.6) to record the total average error TAE. Below is a plot of the recorded predictions over the entire 45 minutes utilizing a sampling window of 15 seconds to predict the next 25 seconds under a delay of 10 seconds.

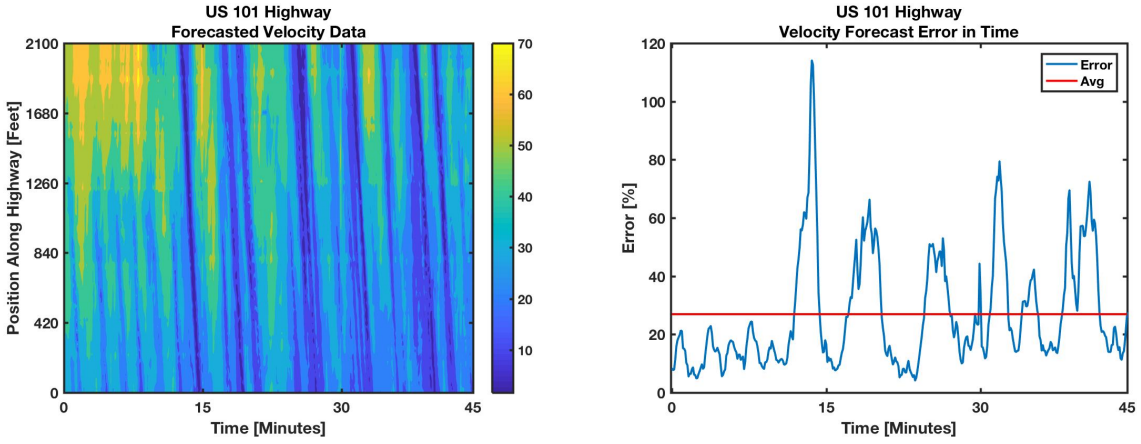

(a) Forecasted Data (b) Error in Time of Forecast

Figure 5.3: US 101 Highway Entire Forecast

5.2 Forecasting of PeMS Data

The previous application of the forecasting methodology to the NGSIM data was primarily intended for illustration. The primary reason being that the NGSIM data exists for only 45 minutes and for very short segments of only two highways. On the other hand, the Caltrans PeMs data set provides years of historical data for hundreds of highways across California. Additionally, the PeMs data set comes from a real-time continuously operating source whereas the NGSIM comes from a one-time recorded experiment. First, a 100 mile stretch of the eastbound US I-10 highway for the week of 3/6/2017-3/12/2017 is studied. The 100 mile section of highway begins near Santa Monica beach in Los Angeles County and ends just passed the city of Beaumont in Riverside County. We use the last 15 minutes of data to predict the next 15 minutes of data utilizing a delay of ten minutes. Simulating over the entire week and recording the predictions made yields the predicted data shown below in figure 5.4b, where the raw data is also plotted for reference.

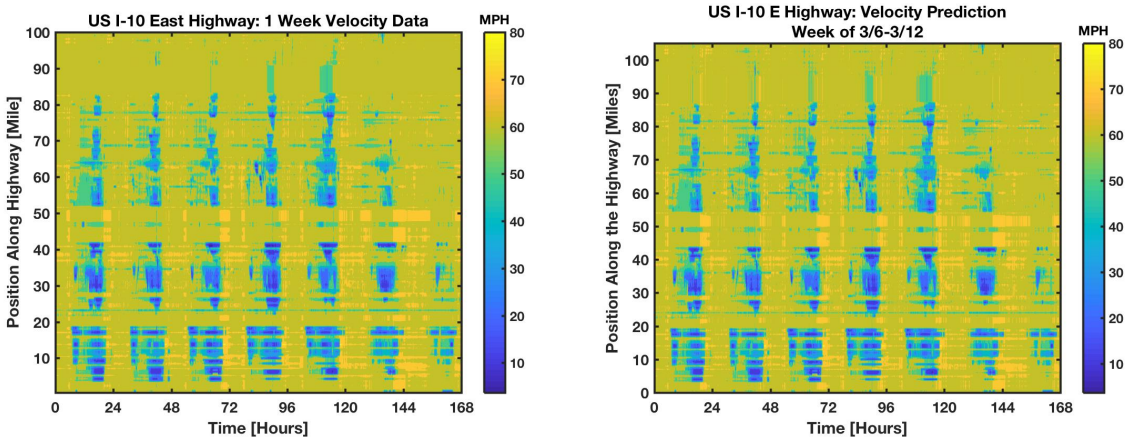

(a) Raw Data (b) Predicted data

Figure 5.4: US I-10 Highway 3/06/2017-3/12/2017

The predictions seem to be in good agreement with the raw data, figure 5.5 below

helps identify the error over the entire week. Together is a plot of the total average error at every time step which can help identify how the error evolves through the week. Figures 5.5a-5.5b confirm that the highest amount of error is obtained during times of traffic congestion. Again, the error can be seen to be very localized about the traffic jams.

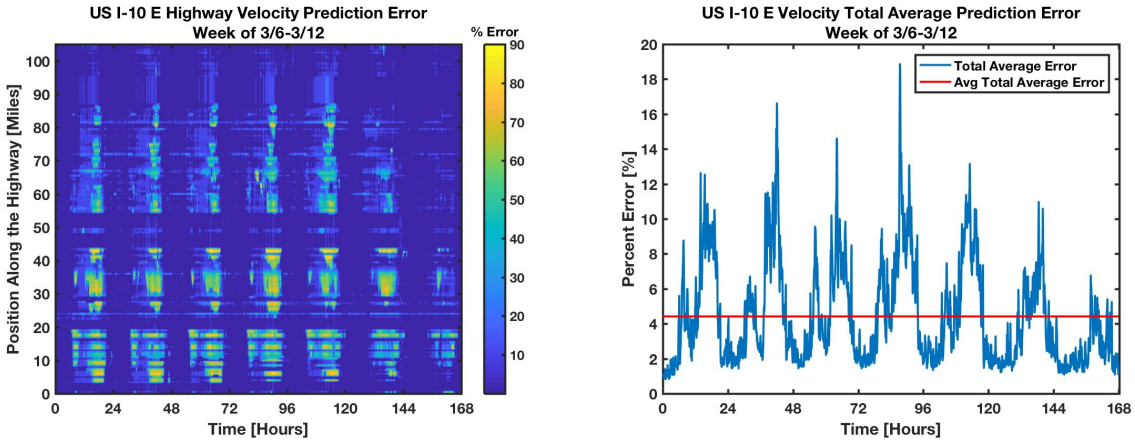

(a) Prediction Error for the Week

(b) Total Average Error vs Time

Figure 5.5: US I-10 Highway 3/06/2017-3/12/2017

We now repeat the previous study for one month's data (March 2017) of a 400 mile stretch of the northbound US I-5 highway. Again, we use the last 15 minutes to predict the next 15 minutes, take a delay of 10 minutes. Figures 5.6-5.7 summarize our raw data, predicted data, and the error in our prediction.

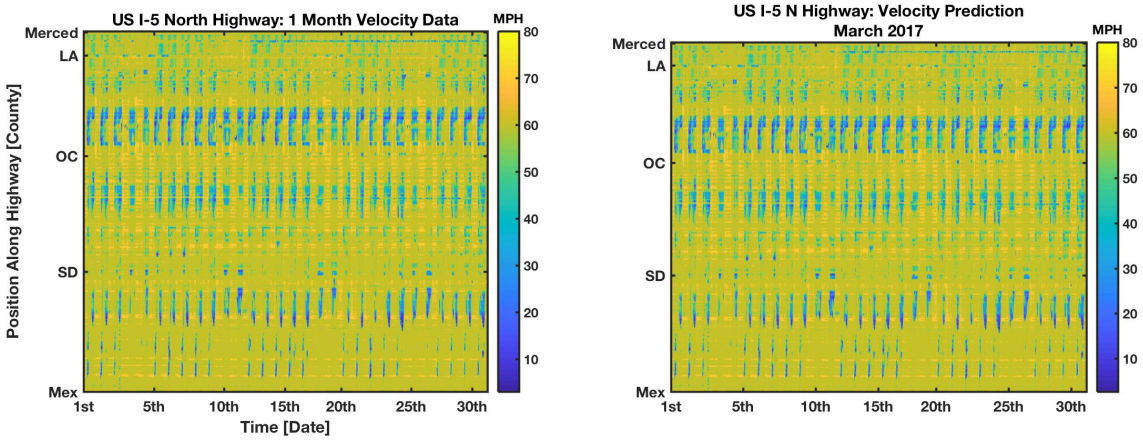

(a) Raw Data (b) Predicted data

Figure 5.6: US I-5 Highway March 2017

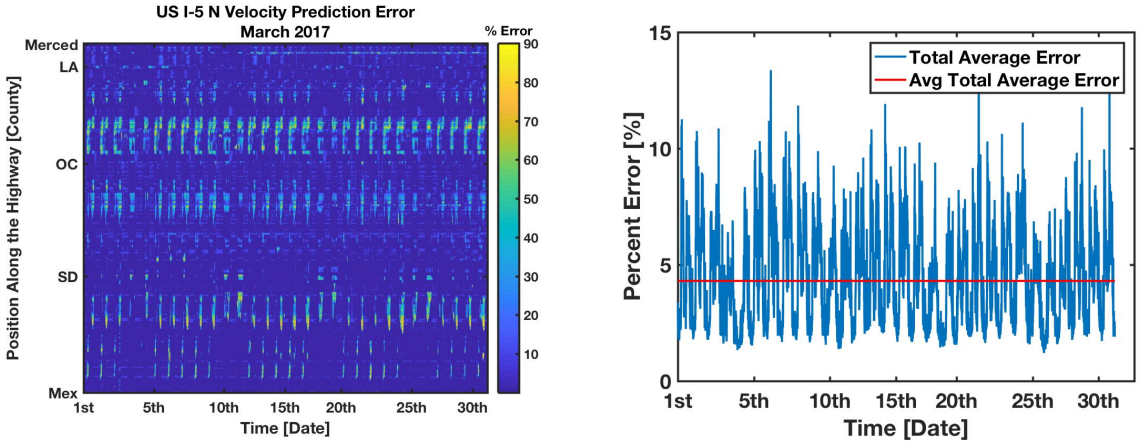

(a) Prediction Error for the Week (b) Total Average Error vs Time

Figure 5.7: US I-5 Highway March 2017

We now investigate how our error varies for different choices of sampling and prediction window, by simulating our predictions for values of (s, p) that are multiples of 15 minutes. For every choice of (s, p) we test how our method performs under a delay of $s - 1$ by recording the average of the TAE, the results are plotted below in figure 5.8. It is evident and intuitive that our error will increase with longer prediction windows.

However, a counter-intuitive aspect of figure 5.8 is that increasing the size of the sampling window only seems to hinder our predictions. This increase in error is seen even for the smallest simulated prediction window of 15 minutes. Overall, figure 5.8 implies that the accurate prediction of traffic is mostly dependant on the most current traffic conditions.

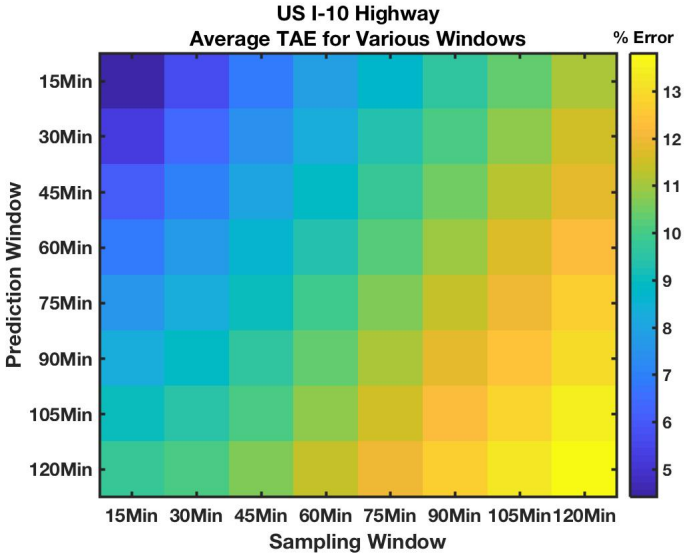

Figure 5.8: Error in Prediction for Various (s, p)

Lastly, we show how our forecasting scheme is not only stable under holiday traffic but also demonstrates how easily it can be extended to cover a network of highways. For this simple, proof of concept, example we will forecast 70 miles of the southbound I-405, eastbound I-210 and the northbound I-110 highways in Los Angeles. The data collected is for the five days of December 22, 2016 - December 26, 2016. Forecasting the network is as simple as stacking the data matrices into one tall matrix, much like in section 4, and then applying the KMD. A plot of the raw data along with the forecasted data is shown below in figures 5.9 and 5.10

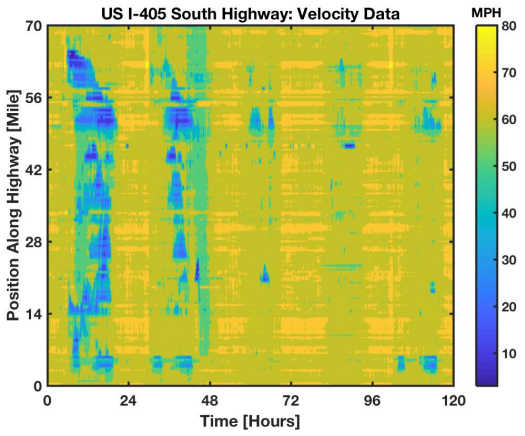

(a) US I-405 South Raw Data

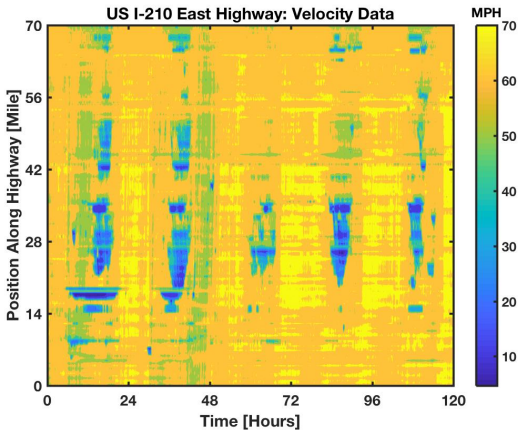

(b) US I-210 East Raw Data

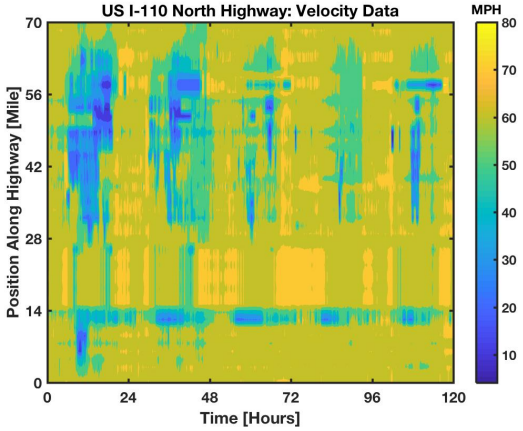

(c) US I-110 East Raw Data

Figure 5.9: Raw Velocity Data for Dec 22, 2016 - Dec 26, 2016

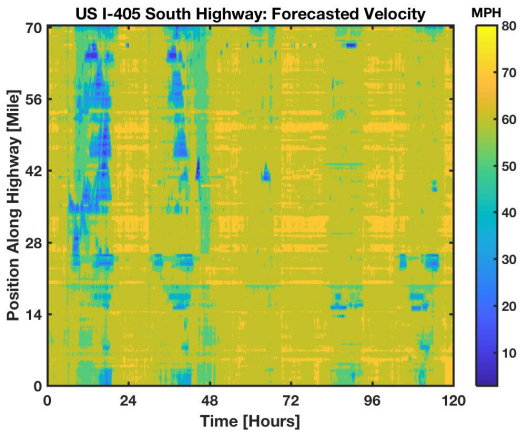

(a) US I-405 South Forecasted Data

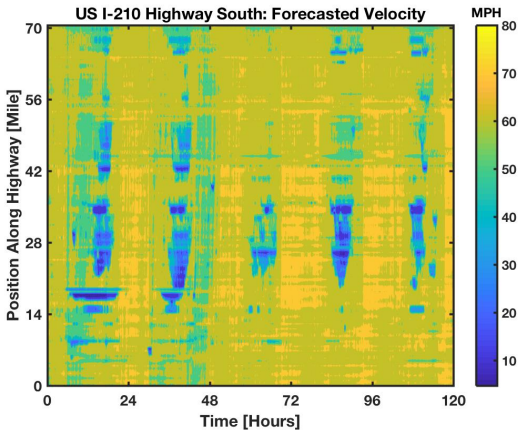

(b) US I-210 East Forecasted Data

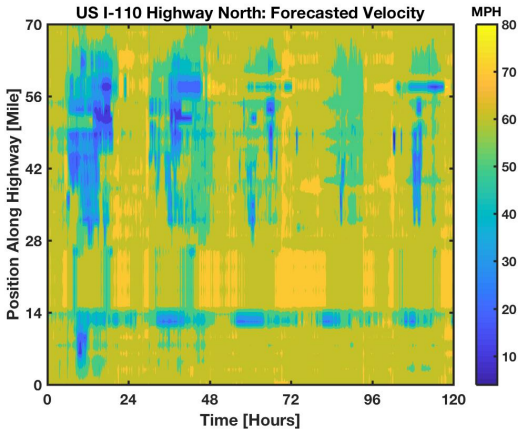

(c) US I-110 East Forecasted Data

Figure 5.10: Forecasted Velocity Data for Dec 22, 2016 - Dec 26, 2016

The percent error matrices and the time evolution of the TAE are plotted together below in figure 5.11. It is evident, that our forecasting scheme remains stable when analyzing a network of highways during the Christmas rush of 2016.

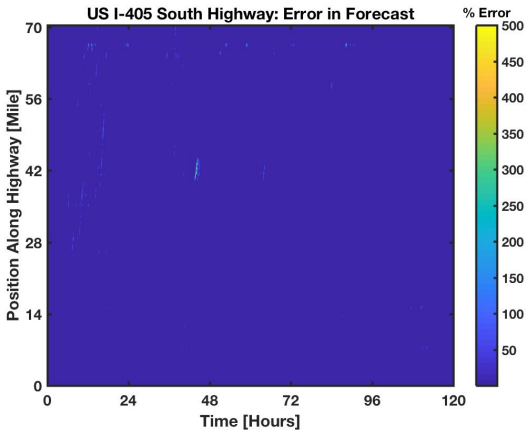

(a) US I-405 South Error in Forecasted Data

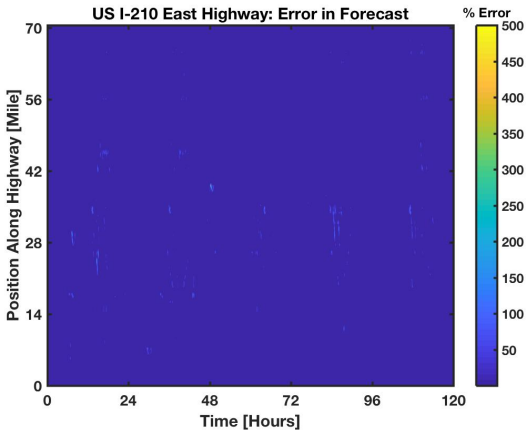

(b) US I-210 East Error in Forecasted Data

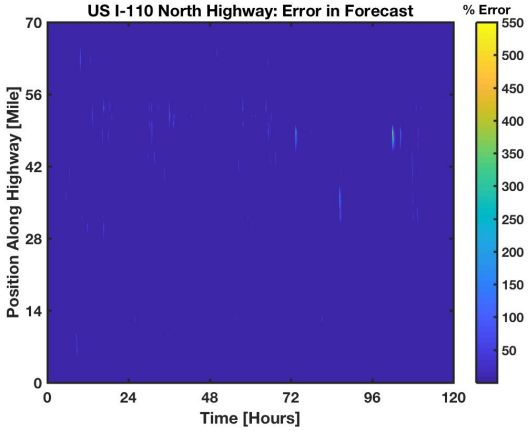

(c) US I-110 East Error in Forecasted Data

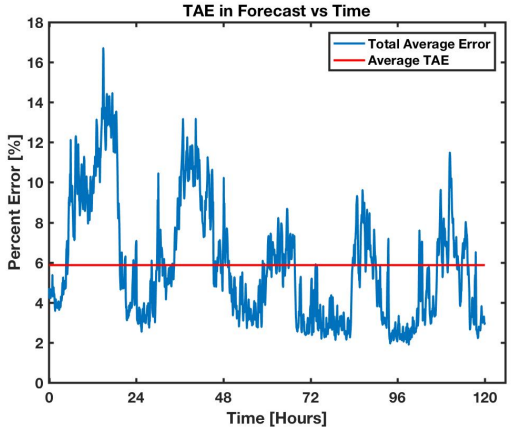

(d) Total Average Error vs Time for Network

Figure 5.11: Forecasted Velocity Data for Dec 22, 2016 - Dec 26, 2016

Chapter 6

Conclusion

It is generally accepted that the applicability of a certain traffic model is dependant on the level of detail required. In this view, microscopic models are typically suitable for the off-line study of merging and linking properties of highway infrastructure, the study of geographical effects on traffic or travel time estimation. The GKT models seem to possess a more theoretical use by yielded a link between microscopic and macroscopic modeling [33]-[37]. Macroscopic models have proven to be useful for the forecast and control of traffic. The inherent limitation with the model or AI-based methods is their lack of universality and need for extensive training data. We have proposed a method based on the spectral properties of the Koopman operator which evidently distinguishes the different states of traffic, identifies any pinned or localized clustering phenomena (modes 1-3), identifies the proposed the pumping effect (modes 4 9). When applied to individual lane data the KMD accurately captures the merging and diverging effects of on/off-ramps and the lane changing effects which give rise to modes with combined lateral and longitudinal (zig-zag) travel. Our methodology provides an objective manner of extracting the associated time and growth scales of traffic patterns. Furthermore, the hierarchy of spatiotemporal patterns obtained can be superimposed to obtain a reconstruction of the observed data. The KMD is capable of achieving this, in a robust manner, without the need for tuning parameters or filtering/smoothing data.

Ultimately, the accurate analysis and prediction of traffic can greatly improve the current control schemes of on-ramp and street metering algorithms. The accurate forecasting of traffic oscillations will lead to retrofitting of highway on-ramp metering algorithms. These static controllers can be programmed to adjust their metering rate so that the oscillation of the traveling wave is dampened as it travels by. Additionally, the accurate forecasting of traffic can lead to the improvement of travel-time estimation algorithms and city holiday planning. The combination of these outcomes will further lead to reduced fuel consumption, travel time and emissions. However, many of the state of the art techniques still lack the ability to reliably and universally forecast traffic. In this work, we have shown how the KMD can offer a parameter-free data-driven platform for the forecasting of traffic. Future works, lie in the direction of better understanding the spikes in error present under heavy traffic conditions, applying the KMD forecasting method to larger street traffic networks, extending these methods to microscopic trajectory data for travel time estimations.

Appendix A

Additional Figures

A.1 NGSIM Reconstruction

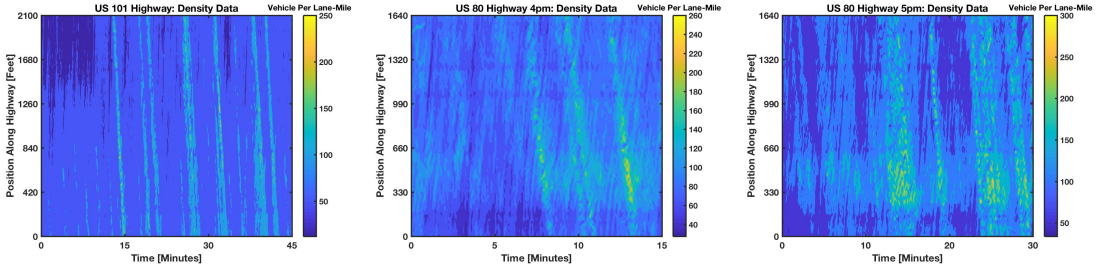

(a) US 101 Highway (b) US 80 Highway 4pm (c) US 80 Highway 5pm

Figure A.1: Density Raw Data

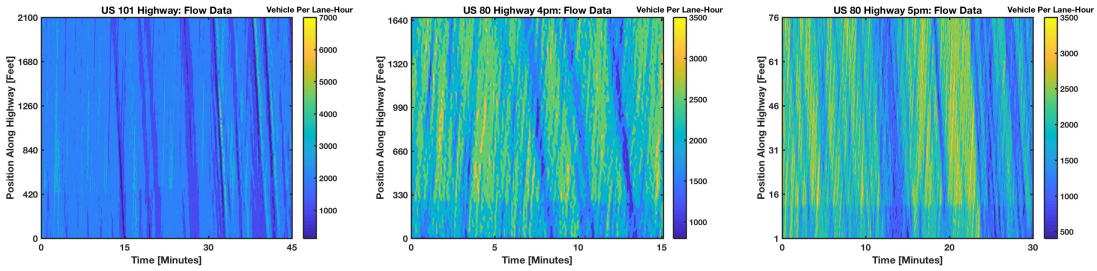

(a) US 101 Highway (b) US 80 Highway 4pm (c) US 80 Highway 5pm

Figure A.2: Flow Raw Data

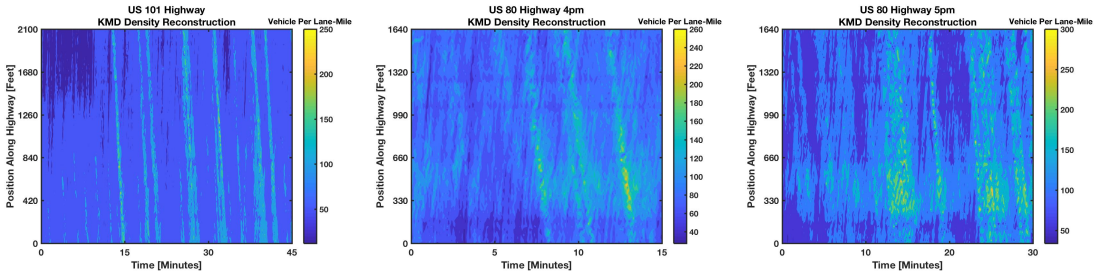

(a) US 101 Highway (b) US 80 Highway 4pm (c) US 80 Highway 5pm

Figure A.3: KMD Density Reconstruction

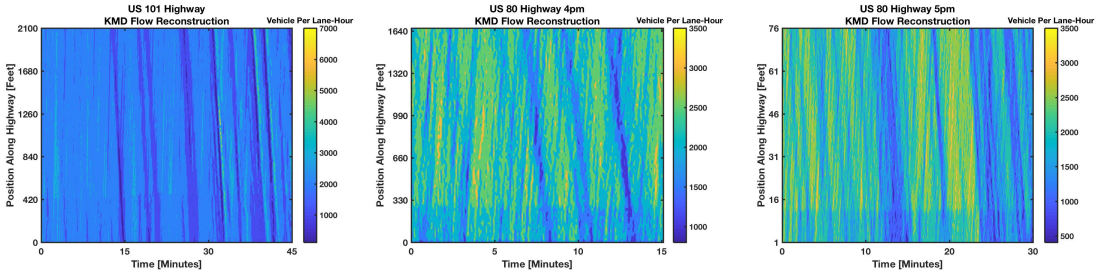

(a) US 101 Highway (b) US 80 Highway 4pm (c) US 80 Highway 5pm

Figure A.4: KMD Flow Reconstruction

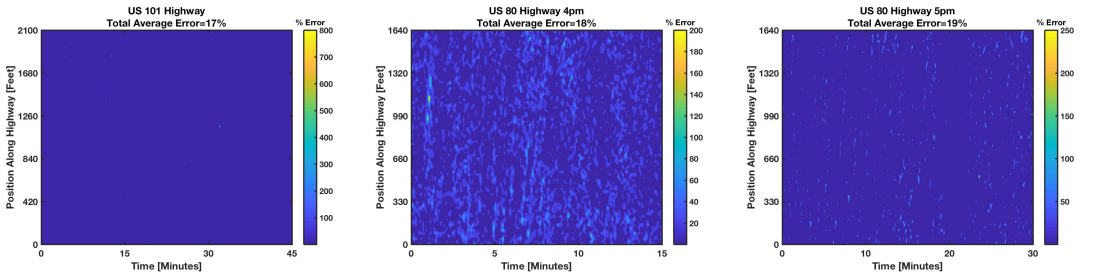

(a) US 101 Error (b) US 80 4m Error (c) US 80 5pm Error

Figure A.5: KMD Density Reconstruction Error

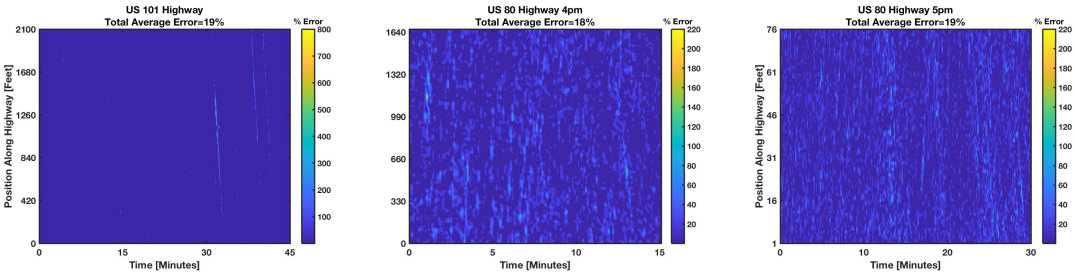

(a) US 101 Error (b) US 80 4pm (c) US 80 5pm

Figure A.6: KMD Flow Reconstruction Error

Bibliography

[1] Aron, M. (1988). Car following in an urban network: Simulation and experiments. Proceedings of Seminar D, 16th PTRC meeting, Bath, Somerset, England, UK, pp. 2739.

[2] Bando, M., Hasebe, K., Nakayama, A., Shibata, A., & Sugiyama, Y. (1995). Dynamical model of traffic congestion and numerical simulation. Physical Review E, 51(2), 10351042.

[3] Brackstone, M., & McDonald, M. (1999). Car-following: A historical review. Transportation Research Part F, 2(4), 181196.

[4] Bullen, A. G. R. (1982). Development of compact micro-simulation for analysing freeway operations and design. Transportation Research Record: Journal of Transportation Research Board, 841, 1518.

[5] Burnham, G. O., & Bekey, G. A. (1976). A heuristic finite state model of the human driver in a car following situation. IEEE Transactions on Systems, Man and Cybernetics SMC, 6(8), 554562.

[6] Chandler, R. E., Herman, R., & Montroll, E. W. (1958). Traffic dynamics: Studies in car following. Operations Research, 6(2), 165184.

[7] Hoefs, D. H. (1972). Entwicklung einer Messmethode uber den Bewegungsablauf des Kolonnenverrkehrs. Germany: Universitat (TH) Karlsruhe.

[8] Helly, W. (1959). Simulation of bottlenecks in single lane traffic flow. Proceedings of the symposium on theory of traffic flow, Research Laboratories, General Motors, New York, pp. 207238.

[9] Treiber, M., Hennecke, A., & Helbing, D. (2000). Congested traffic states in empirical observations and microscopic simulations. Physical Review E, 62(2), 18051824.

[10] Pipes, L. A. (1953). An operational analysis of traffic dynamics. Journal of Applied Physics, 24(3), 274281

[11] Kometani, E., & Sasaki, T. (1959). Dynamic behavior of traffic with a nonlinear spacing-speed relationship. Proceedings of the symposium on theory of traffic flow, Research Laboratories, General Motors, New York, pp. 105119.

[12] Gipps, P. G. (1981). A behavioral car following model for computer simulation. Transportation Research B, 15(2), 105111.

[13] Michaels, R. M. (1963). Perceptual factors in car following. Proceedings of the second international symposium on the theory of road traffic flow, Paris, pp. 4459.

[14] Michaels, R. M., & Cozan, L. W. (1963). Perceptual and field factors causing lateral displacements. Public Roads, 32, 233240.

[15] Wiedemann, R. (1974). Simulation des Strassenverkehrsflusses. Technical report, Institut fur Verkehrswesen, Universitat Karlsruhe, Karlsruhe, Germany, In German.

[16] Espie, S., Saad, F., Schnetzler, B., Bourlier, F., & Djemame, N. (1994). Microscopic traffic simulation and driver behavior modelling: The ARCHISIM project. The Strategic Highway Research Program and Traffic Safety on Two Continents, Lille, France.

[17] Kikuchi, C., & Chakroborty, P. (1992). Car following model based on a fuzzy inference system. Transportation Research Record: Journal of the Transportation Research Board, 1365, 8291.

[18] McDonald, M., Wu, J., & Brackstone, M. (1997). Development of a fuzzy logic based microscopic motorway simulation mode. Proceedings of the ITSC97 conference, Boston, USA.

[19] Hongfei, J., Zhicai, J., & Anning, N. (2003). Develop a car-following model using data collected by five-wheel system. Proceedings of the IEEE intelligent transportation system, Vol. 1, China, pp. 346351.

[20] Panwai, S., & Dia, H. (2007). Neural agent car-following models. IEEE Transactions on Intelligent Transportation Systems, 8(1), 6070

[21] Kayvan Aghabayk, Majid Sarvi & William Young (2015) A State-of-the-Art Review of Car-Following Models with Particular Considerations of Heavy Vehicles, Transport Reviews, 35:1, 82-105, DOI: 10.1080/01441647.2014.997323

[22] S. P. Hoogendoorn, P. H. L. Bovy, "State-of-the-Art of Vehicular Traffic Flow Modeling", J. Sys. and Control Eng., vol. 215, no. 4, pp. 283-304, Aug. 2001.

[23] Brackstone, M., & McDonald, M. (1999). Car-following: A historical review. Transportation Research Part

[24] M. Schonhof, D. Helbing, Empirical features of congested traffic states and their implications for traffic modeling, cond-mat/0408138.

[25] Li, S. (2003). Simulation of car-following decision using fuzzy neural network system. Proceedings of the IEEE international conference on intelligent transportation system, Vol. 1, pp. 140145.

[26] Ma, X. (2004). Toward an integrated car-following and lane-changing model based on neural-fuzzy approach. Helsinki summer workshop, Centre for Traffic Research, Stockholm.

[27] Botma, H. (1978), State-of-the-Art report Traffic Flow Models (in Dutch). Research Report R-78- 40, SWOV.

[28] Prigogine, I., & R. Herman (1971). Kinetic Theory of Vehicular Traffic. American Elsevier New- Y ork.

[29] Paveri-Fontana, S.L. (1975). On Boltzmann-Like treatments for traffic flow: a critical review of the basic model and an alternative proposal for dilute traffic analysis. Transportation Research B 9, 225-235.

[30] Helbing, D. (1997b). Modeling Multi-lane Traffic Flow with Queuing Effects. Physica A 242, 175- 194.

[31] Hoogendoorn, S.P., & P.H.L. Bovy. (2000b). Modelling Multiple User-Class Traffic Flow. Transportation Research B (34)2, 123-146.

[32] Hoogendoorn, S.P. (1999). Multiclass Continuum Modelling of Multiclass Traffic Flow. PhD. Thesis T99/5. TRAIL Thesis Series, Delft University Press.

[33] Helbing, D. (1996). Gas-kinetic derivation of Navier-Stokes-like traffic equations. Physical Review E 53(3), 2266-2381.

[34] Helbing, D. (1997a). Fundamentals of traffic flow. Phys. Rev. E 55 3735-3738.

[35] Helbing, D. (1997b). Modeling Multi-lane Traffic Flow with Queuing Effects. Physica A 242, 175- 194.

[36] Klar, A., and Wegener (1998), A Hierarchy of Models for Multilane Vehicular Traffic I II: Model- ling. SIAM Journal of Applied Mathematics.

[37] Hoogendoorn, S.P. (1999). Multiclass Continuum Modelling of Multiclass Traffic Flow. PhD. Thesis T99/5. TRAIL Thesis Series, Delft University Press.

[38] Hoogendoorn, S.P. and P.H.L. Bovy (2000a). Gas-Kinetic Modeling and Simulation of Pedestrian Flows. To appear in Transportation Research Board 2000. TRB-paper 00-1662

[39] Lighthill, M.H., and G.B. Whitham (1955). On kinematic waves II: a theory of traffic flow on long, crowded roads. Proceedings of the Royal Society of London series A, 229, 317-345.

[40] Payne, H.J. (1971). Models for Freeway Traffic and Control. In: Bekey, G.A. (ed), Mathematical Models of Public Systems 1, 51-61.

[41] Payne, H.J. (1979). FREFLO: A Macroscopic Simulation Model of Freeway Traffic. Transportation Research Record 722, 68-77.

[42] A. Aw and M. Rascle, Resurrection of second order models of traffic flow, SIAM Journal on Applied Mathematics, vol. 60, no. 3, pp. 916938, 2000.

[43] H.M. Zhang. A non-equilibrium traffic model devoid of gas-like behavior. Transportation Research Part B: Methodological, 36(3):275 290, 2002.

[44] Munoz, J. C, C. F. Daganzo. 2003. Structure of the transition zone behind freeway queues. Transportation Sci. 37 312-329.

[45] Nagel, K., P. Nelson. 2005. A critical comparison of the kinematic wave model with observational data. H. S. Mahmassani, ed. Proc. 16th Internat. Sympos. Transportation Traffic Flow Theory, Elsevier, Amsterdam, The Netherlands, 145-163.

[46] Daganzo, C. F. 1995b. Requiem for second-order fluid approxima tions of traffic flow. Transportation Res. Part B 29 277-286.

[47] M. Schonhof, D. Helbing, Empirical features of congested traffic states and their implications for traffic modeling, cond-mat/0408138

[48] Ahn, S. (2005). Formation and spatial evolution of traffic oscillations. Doctoral Dissertation, Department of Civil and Environment Engineering, University of California, Berkeley.

[49] Ahn, S. Cassidy, M.J. (2007). Freeway traffic oscillations and vehicle lane-change maneuvers. Proceedings of the 17Th International Symposium on Transportation and Traffic Theory, Amsterdam, Elsevier, 691-710.

[50] Edie, L. C, E. Baverez. 1965. Generation and propagation of stop start traffic waves. L. Edie, R. Herman, R. Rothery, eds. Vehicu lar Traffic Science, Proc. 3rd Internat. Sympos. Theory Traffic Flow, New York, 26-37.

[51] Mika, H. S., J. B. Kreer, L. S. Yuan. 1969. Dual mode behavior of freeway traffic. Highway Res. Record 279 1-13.

[52] Koshi, M., M. Iwasaki, I. Ohkura. 1983. Some findings and an overview on vehicular flow characteristics. V. F. Hur dle, E. Hauer, G. N. Stewart, eds. Proc. 8th Internat. Sympos. Transportation Traffic Flow Theory, University of Toronto Press, Toronto, Ontario, 403-426.

[53] Kuhne, R. D. 1987. Freeway speed distribution and acceleration noise?calculations from a stochastic continuum theory and comparison with measurements. N. H. Gartner, N. H. M. Wilson, eds. Proc. 10th Internat. Sympos. Transportation Traffic Theory. Elsevier, New York, 119-137.

[54] Helbing, D. 1997c. Traffic data and their implications for consis tent traffic flow modeling. M. Papageorgiou, A. Pouliezos, eds. Transportation Systems. International Federation of Automatic Control, Chania, Greece, 809-814.

[55] Kerner, B. S., 1998a, Phys. Rev. Lett. 81, 3797

[56] Kerner, B. S., H. Rehborn. 1996a. Experimental features and char acteristics of traffic jams. Phys. Rev. E 53 R1297-R1300.

[57] Kerner, B. S. 2000a. Phase transitions in traffic flow. D. Helbing, H. J. Herrmann, M. Schreckenberg, D. E. Wolf, eds. Proc. Traffic Granular Flow '99: Social, Traffic and Granular Dynamics. Springer, Berlin, Germany, 253-284.

[58] Kerner, B. S. 2000b. Theory of breakdown phenomenon at highway bottlenecks. Transportation Res. Record 1710 136-144.

[59] Cassidy, M. J., M. Mauch. 2001. An observed traffic pattern in long freeway queues. Transportation Res. Part A 35 143-156.

[60] Windover, J. R. 1998. Empirical studies of the dynamic features of freeway traffic. Ph.D. thesis, University of California, Berkeley, CA.

[61] Mimoz, J. C, C. F. Daganzo. 1999. Experimental observations upstream of an active bottleneck caused by a freeway off-ramp. PATH working paper, California Partners for Advanced Tran sit and Highways, Richmond, CA.

[62] Ahn, S., Laval, J.A., Cassidy, M.J. (2010). Merging and diverging effects on freeway traffic oscillations: theory and observations. Transportation Research Record, Journal of the Transportation Research Board, 2188,1-8.

[63] Laval, J. A., C. F. Daganzo. 2006. Lane-changing in traffic streams. Transportation Res. Part B 40 251-264.

[64] Wilson, R. E. 2008 Mechanisms for spatio-temporal pattern formation in highway traffic models. Phil. Trans. R. Soc. A 366, 20172032. (doi:10.1098/rsta.2008.0018)

[65] Laval, J. A. Leclercq, L. 2010 A mechanism to describe the formation and propagation of stop-and-go waves in congested freeway traffic. Phil. Trans. R. Soc. A 368, 45194541. (doi:10.1098/rsta.2010.0138)

[66] Daganzo, C. E 2002b. A behavioral theory of multi-lane trafficflow. II: Merges and the onset of congestion. Transportation Res. Part B 36 159-169.

[67] Mauch, M., M. J. Cassidy. 2002. Freeway traffic oscillations: Observations and predictions. M. A. P. Taylor, ed. Proc. 15th Inter nat. Sympos. Traffic Transportation Theory, Elsevier, Amsterdam, The Netherlands, 653-674.

[68] B. Zielke, R. Bertini, M. Treiber, Empirical Measurement of Freeway Oscillation Characteristics: An International Comparison, Transportation Research Record 2088, 57 (2008)

[69] Treiber, M. and D. Helbing. An adaptive smoothing method for traffic state identification from incomplete information. In: Interface and transport dynamics: Computational Modelling. Berlin: Springer, 2003, 343360 (see p. 7).

[70] Lindgren, R. V. F. Analysis of Flow Features in Queued Traffic on a German Freeway. PhD dissertation. Portland State University, Oregon, 2005.

[71] Mauch, M. Analysis of Start-Stop Waves in Congested Freeway Traffic. PhD dissertation. University of California, Berkeley, 2002.

[72] Leal, M. T. Empirical Analysis of Traffic Flow Features of a Freeway Bottleneck Surrounding a Lane Drop. MS thesis. Portland State University, Oregon, 2002.

[73] Bertini, R. L., and M. T. Leal. Empirical Study of Traffic Features at a Freeway Lane Drop. Journal of Transportation Engineering, Vol. 131, No. 6, 2005, pp. 397407.

[74] L. C. Edie, Discussion of traffic stream measurements and definitions, in Proc. 2nd Int. Symp. on the Theory of Traffic Flow, pp. 139 154, 1963.

[75] B. Piccoli, K. Han, T. L. Friesz, T. Yao, and J. Tang, Second-order models and traffic data from mobile sensors, Transp. Res. C, vol. 52, pp. 3256, 2015.

[76] F. Takens (1981). "Detecting strange attractors in turbulence". In D. A. Rand and L.-S. Young. Dynamical Systems and Turbulence, Lecture Notes in Mathematics, vol. 898. Springer-Verlag. pp. 366381

[77] B. M. Williams and L. A. Hoel, Modeling and forecasting vehicular traffic flow as a seasonal ARIMA process: Theoretical basis and empirical results, J. Transp. Eng., vol. 129, no. 6, pp. 664672, Nov./Dec. 2003.

[78] Tan, M.-C., Wong, S.C., Xu, J.-M., Guan, Z.-R., Zhang, P., 2009. An aggregation approach to short-term traffic flow prediction. IEEE Transactions on Intelligent Transportation System 10 (1), 6069.

[79] T. Sauer, J. A. Yorke, M. Casdagli, Embedology, J. Stat. Phys. 65 (34) (1991) 579616. doi:10.1007/bf01053745.

[80] J. C. Robinson, A topological delay embedding theorem for infi- nite-dimensional dynamical systems, Nonlinearity 18 (5) (2005) 21352143. doi:dx.doi.org/10.1088/0951-7715/18/5/013.

[81] E. R. Deyle, G. Sugihara, Generalized theorems for nonlinear state space reconstruction, PLoS ONE 6 (3) (2011) e18295. doi:10.1371/journal.pone.0018295.

[82] Vlahogianni, E.I., Karlaftis, M.G., Golia, J.C., 2014. Short-term traffic forecasting: where we are and where were going. Transport. Res. Part C 43 (1), 319

[83] Gartner, N., C. J. Messer, and A. K. Rathi. Traffic Flow Theory: A State- of-the-Art Report, Revised Monograph on Traffic Flow Theory. www.tfhrc. gov/its/tft/tft.htm.

[84] Kim, T., and H. M. Zhang. Gap Time and Stochastic Wave Propagation. Proc., IEEE 7th Annual Conference on Intelligent Transportation Systems, Washington, D.C., 2004.

[85] Badhrudeen, M., Raj, J., Vanajakshi, L. D. (2016). Shortterm prediction of traffic parametersperformance comparison of a datadriven and lessdatarequired approaches. Journal of Advanced Transportation, 50(4), 647-666.

[86] Barros, J., Araujo, M., Rossetti, R. J. (2015, June). Short-term real-time traffic prediction methods: A survey. In Models and Technologies for Intelligent Transportation Systems (MT-ITS), 2015 International Conference on (pp. 132-139). IEEE.

[87]] B. O. Koopman, Proceedings of the National Academy of Sciences 17, 315 (1931).

[88] B. O. Koopman and J. von Neumann. Dynamical systems of continuous spectra. Proceedings of the National Academy of Sciences of the United States of America, 18(3):255, 1932.

[89] I. Mezic and A. Banaszuk, Physica D: Nonlinear Phenomena 197, 101 (2004).

[90] Igor Mezic. Spectral properties of dynamical systems, model reduction and decompositions. Nonlinear Dynamics, 41(1-3):309325, 2005.

[91] Hassan Arbabi and Igor Mezic. Study of dynamics in unsteady flows using koopman mode decomposition. arXiv preprint arXiv:1704.00813, 2017.

[92] I. Mezic . Analysis of fluid flows via spectral properties of Koopman operator. Annual Review of Fluid Mechanics, 45, January 2013.

[93] Marko Budivsic, Ryan Mohr, and Igor Mezic. Applied koopmanism a). Chaos: An Interdisciplinary Journal of Nonlinear Science, 22(4):047510, 2012.

[94] Alexandre Mauroy and Igor Mezic . On the use of fourier averages to compute the global isochrons of (quasi) periodic dynamics. Chaos: An Interdisciplinary Journal of Nonlinear Science, 22(3):033112, 2012.

[95] Yoshihiko Susuki and Igor Mezic. Nonlinear koopman modes and coherency identification of coupled swing dynamics. IEEE Transactions on Power Systems, 26(4):18941904, 2011.

[96] Alexandre Mauroy and Igor Mezic. Global stability analysis using the eigenfunctions of the koopman operator. 2014.

[97] Igor Mezic. On applications of the spectral theory of the koopman operator in dynamical systems and control theory. In Decision and Control (CDC), 2015 IEEE 54th Annual Conference on, pages 70347041. IEEE, 2015.

[98] Bingni W Brunton, Lise A Johnson, Jeffrey G Ojemann, and J Nathan Kutz. Extracting spatialtemporal coherent patterns in large-scale neural recordings using dynamic mode decomposition. Journal of neuroscience methods, 258:115, 2016.

[99] Steven L Brunton, Bingni W Brunton, Joshua L Proctor, Eurika Kaiser, and J Nathan Kutz. Chaos as an intermittently forced linear system. arXiv preprint arXiv:1608.05306, 2016.

[100] Steven L Brunton, Bingni W Brunton, Joshua L Proctor, and J Nathan Kutz. Koopman invariant subspaces and finite linear representations of nonlinear dynamical systems for control. PloS one, 11(2):e0150171, 2016.

[101] Steven L Brunton, Joshua L Proctor, and J Nathan Kutz. Compressive sampling and dynamic mode decomposition. arXiv preprint arXiv:1312.5186, 2013.

[102] D. Giannakis, J. Slawinska, and Z. Zhao. Spatiotemporal feature extraction with data-driven koopman operators. In Proceedings of The 1st International Workshop on Feature Extraction: Modern Questions and Challenges, NIPS, pages 103115, 201

[103] M. Korda and I. Mezic. Linear predictors for nonlinear dynamical systems: Koopman operator meets model predictive control. arXiv preprint arXiv:1611.03537, 2016.

[104] Moridpour S, Sarvi M, Rose G. Lane changing models: a critical review. Transportation Letters: The International Journal of Transportation Research 2010; 2(3): 157173.

[105] P. Schmid and J. Sesterhenn. Dynamic mode decomposition of numerical and experimental data. In In Sixty-First Annual Meeting of the APS Division of Fluid Dynamics, 2008.

[106] C.W. Rowley, I. Mezic , S. Bagheri, P. Schlatter, and D.S. Henningson. Spectral analysis of nonlinear flows. Journal of Fluid Mechanics, 641(1):115127, 2009.

[107] Giannakis, D. 2016 Data-driven spectral decomposition and forecasting of ergodic dynamical systems. ArXiv: 1507.02338v2.

[108] Yoshihiko Susuki and Igor Mezic. A prony approximation of koopman mode decomposition. In 2015 54th IEEE Conference on Decision and Control (CDC), pages 70227027. IEEE, 2015.

[109] Matthew O Williams, Ioannis G Kevrekidis, and Clarence W Rowley. A data-driven approximation of the koopman operator: Extending dynamic mode decomposition. Journal of Nonlinear Scence, 25(6):13071346, 2015

[110] M. O. Williams, C. W. Rowley, and I. G. Kevrekidis. A kernel approach to data-driven Koopman spectral analysis. http://arxiv.org/abs/1411.2260, 2014.

[111] J Nathan Kutz, Xing Fu, and Steven L Brunton. Multiresolution dynamic mode decomposition. SIAM Journal on Applied Dynamical Systems, 15(2):713735, 2016.

[112] Joshua L Proctor, Steven L Brunton, and J Nathan Kutz. Dynamic mode decomposition with control. SIAM Journal on Applied Dynamical Systems, 15(1):142161, 2016

[113] Igor Mezic. Koopman operator spectrum and data analysis. arXiv preprint arXiv:1702.07597, 2017.

[114] Korda, M. Mezic, I. 2017 On convergence of Extended Dynamic Mode Decomposition to the Koopman operator. ArXiv: 1703.04680v3.

[115] Jonathan H Tu, Clarence W Rowley, Dirk M Luchtenburg, Steven L Brunton, and J Nathan Kutz. On dynamic mode decomposition: theory and applications. Journal of Computational Dynamics, 1:391421, 2014.

[116] H. Arbabi and I. Mezic. Ergodic theory, dynamic mode decomposition and computation of spectral properties of the koopman operator. arXiv preprint arXiv:1611.06664, 2016